Supporting Materials

Novel Multicomponent Crystal Forms of Artesunate

Shadrack J. Madu[1], Ke Wang[1], László Fábián[2], and Mingzhong Li[1*]

[1]School of Pharmacy, De Montfort University, Leicester LE1 9BH, U.K.

[2]School of Chemistry, Pharmacy and Pharmacology, University of East Anglia, Norwich Research Park, Norwich NR4 7TJ, U.K.

Table S1: List of coformers screened

[*] Corresponding author: Professor Mingzhong Li, email: mli@dmu.ac.uk

1,10-phenanthroline (PHEN, 99% purity)	Carbamazepine (CBZ, ≥99% purity)	Ibuprofen (IBP, ≥99% purity)	Paracetamol (PCM, ≥98% purity)
1,11-undecanedicarboxylic acid (UDCA, 92% purity)	Chrysin (CSN, 99+% purity)	Imidazole (IMZ, 99% purity)	Phenazine (PHZ, 98% purity)
1,2-Di(pyridine-4-yl)ethane (DPE, ≥97% purity)	Cinchonidine (CNCD, 98.50101% purity)	Indomethacin (IND, ≥99% purity)	Pimelic acid (PIA, 98% purity)
2,6- dihydro benzoic acid (DHBA, 98% purity)	Cinnamic acid (Trans) (CNA, ≥99% purity)	Isonicotinamide (INA, 99% purity)	Piperazine (PIZ, 99% purity)
2-amino-5-methyl benzoic acid (AMBA, 97% purity)	Citraconic acid (CTA, 99+% purity)	Isonicotinic acid (ISA, 99% purity)	Piracetam (PIR, ≥98% purity)
2-aminopyrazine (APY, ≥99% purity)	Citric acid (CA, 99% purity)	Isoniazid (INH, 99% purity)	Praziquantel (PZQ, ≥98% purity)
2-Aminopyrimidine (AMP, 98% purity)	Climbazole (CLBZ, ≥99% purity)	Itaconic acid (ITCA, 99% purity)	Pthalamide (PTA, ≥97% purity)
2-Ketoglutaric acid (KEA, 98% purity)	Clotrimazole (CTZ, ≥97.5% purity)	Itraconazole (ITZ, 99% purity)	Pyrazinamide (PZA, 99% purity)
2-Picolinic acid (2-PCA, 99% purity)	Curcumin (CUR, ≥98% purity)	Ketoconazole (KCZ, 98% purity)	Pyrazine (PYR, ≥99% purity)
3-Aminopyridine (APR, 99% purity)	Cyclamic acid (CYA, ≥98% purity)	Ketoprofen (KTP, 95% purity)	Pyrogallol (PG, ≥98% purity)
4,4-Bipyridine (BPY, 98% purity)	Cytosine (CYT, ≥98% purity)	Lactose BP (LAC)	Quercetin (QUE, ≥95% purity)
4-aminobenzoic acid (ABA, ≥99% purity)	1,4-Diazabicyclo[2.2.2]octane (DABCO, 97% purity)	L-arginine (ARG, ≥98% purity)	Ranitidine (RAN ≥98% purity)
4-hydroxybenzohydrazide (HYB, ≥97% purity)	Daidzein (DAI, 97% purity)	Levetiracetam (LEV, ≥97.5% purity)	Resveratrol (Trans) (RSV, 98% purity)
4-hydroxybenzoic acid (97% purity)	D-Glucoronic acid (D-GlcA, 98+% purity)	L-Glutamic (L-GLUA, ≥99% purity)	Riboflavin (RIB, 98% purity)
5-Fluorouracil (FLU, ≥99% purity)	DL-Tryptophan (TRY, ≥99% purity)	L-Proline (L-PRO, ≥99% purity)	Saccharin (SAC, ≥98% purity)
5-Flurocytosine (5-FC, 99+% purity)	D-Phenylalanine (PHE, ≥98% purity)	L-Tartaric acid (L-TA, 99% purity)	Salicyclic acid (SA, ≥99% purity)
Acetone 1,3-dicarboxylic acid (ACDA, 97% purity)	DL-Proline (DL-PRO, 998% purity)	Luteolin (LUT, >98% purity)	Sebacic acid (SEBA, 98% purity)
Acetophenone oxime (ACO, ≥98% purity)	Ethylene Diamine Tetra Acetic Acid (EDTA)	Maleic acid (MAA, ≥99% purity)	Suberic acid (SUBA, 99% purity)
Adipic acid (ADA, 99% purity)	Etidronic acid (ETA, 96% purity)	Malic acid (MA, 98+% purity)	Succinic acid (SUA, ≥99% purity)
Albendazole (ABZ, 98% purity)	Fluconazole (FLZ, 98% purity)	Mebendazole (MBZ, >95% purity)	Terephthalic acid (TPA, 98+% purity)
Amodiaquine 2HCL H20 (AQ, ≥97.5% purity)	Flufenamic acid (FFA, ≥97% purity)	Mefenamic acid (MFA, ≥98% purity)	Theophylline (THP, 99+% purity)
Allopurinol (ALO, 98% purity)	Folic acid (FA, 97% purity)	Methenamine (MEA, ≥99% purity)	Theophylline-7-acetic acid (TAA, 98% purity)
Apigenin (APG, 98% purity)	Fumaric Acid (FUMA, ≥99% purity)	Muconic acid (MUCA, 98% purity)	Tolfenamic acid (TFA, ≥98% purity)
Artemisinin (ART, ≥98% purity)	Ganciclovir (GCV, 98% purity)	Nadolol (NAD, ≥ 98% purity)	Urea (URE, 99.5% purity)
Aspartame (ASP-TM, 98% purity)	Glutaric acid (GLA, 99% purity)	Naphthalene-2,6-dicarboxylic acid (NDA, 98% purity)	Voriconazole (VCZ, 98% purity)
Aspirin (ASP, 99% purity)	Glycine (GLY, 99% purity)	Nicotinamide (NIC, ≥99.5% purity)	Xanthine (XAN, 99% purity)
Azelaic acid (AZA, 96% purity)	Hesperetin (HSP, 97% purity)	Nicotinic acid (NA, ≥99.5% purity)	Xylitol (XLT, ≥ 99% purity)
Benzoic acid (BZA, 99.6% purity)	Hippuric acid (HIA, 98% purity)	Niflumic acid (NFA, ≥98% purity)	
Biotin (BTN, 98% purity)	Hydrochlorothiazide (HCT, 95% purity)	Oxalic acid (OA, 99% purity)	
Caffeine (CAF, ≥99% purity)	Hydroxyurea (HU, 98% purity)	Pamoic acid (PMA, 99% purity)	

Table S2: ATS recrystallisation experiments

Solvent	Quantity of sample (mg)	Volume of solvent (mL)	Temperature (°C)	Stirring speed (rpm)
Methanol	100	2	25	200
Ethanol	100	2	25	200
Ethyl acetate	100	2	25	200
Acetonitrile	100	2	25	200
Acetone	100	2	25	200
Propan-2-ol	100	2	25	200
Chloroform	100	4	50	200
Tetrahydrofuran	100	4	50	200
Dichloromethane	100	10	70	200
Toluene	100	10	100	200
Isobutanol	100	2	70	200
Diethyl ether	100	20	30	700
Nitromethane	100	2	70	200
n-Hexane	Insoluble			
n-Heptane	Insoluble			

Table S3: Crystallographic Data for Refinement of ATS Cocrystals/Salts

Identification code	ATS-ABA	ATS^2-DABCO Form 1	ATS^2-DABCO Form 2	ATS-PHEN	ATS-URE-CH_3OH	ATS-URE-C_2H_3N
Empirical formula	C26 H35 N O10	C44 H68 N2 O16	C44 H68 N2 O16	C31 H36 N2 O8	C21 H36 N2 O10	C22 H35 N3 O9
Formula weight	521.55	881.00	881.00	564.62	476.52	485.53
Temperature	100.00 K	99.99(10) K	100.00(10) K	99.98(11) K	100.00(10) K	100 K
Wavelength	1.54184 Å	1.54184 Å	1.54184 Å	1.54184 Å	1.54184 Å	1.54184 Å
Crystal system	Monoclinic	Monoclinic	Monoclinic	Monoclinic	Monoclinic	Monoclinic
Space group	$P2_1$	$P2_1$	$P2_1$	$P2_1$	$P2_1$	$P2_1$
a	5.69290(1) Å	10.3355(2) Å	11.0046(11) Å	9.57054(18) Å	10.3625(5) Å	10.5562(3) Å
b	17.0162(2) Å	10.1548(2) Å	8.5912(8) Å	51.5305(6) Å	7.3357(3) Å	7.3837(2) Å
c	13.4451(2) Å	21.6741(3) Å	23.6155(18) Å	9.8305(2) Å	15.0315(6) Å	15.7892(5) Å
β	96.1350(1)°	102.644(2)°	98.743(9)°	118.766(3)°	93.125(4)°	98.315(3)°
Volume	1294.99(3) $Å^3$	2219.64(7) $Å^3$	2206.7(3) $Å^3$	4249.88(16) $Å^3$	1140.94(9) $Å^3$	1217.73 (6) $Å^3$
Z	2	2	2	6	2	2
Density (calculated)	1.338 g/cm^3	1.318 g/cm^3	1.326 g/cm^3	1.324 g/cm^3	1.387 g/cm^3	1.324 g/cm^3
Absorption coefficient	0.861 mm^{-1}	0.830 mm^{-1}	0.835 mm^{-1}	0.789 mm^{-1}	0.929 mm^{-1}	0.863 mm^{-1}
F(000)	556	948	948	1800	512	520
Crystal size	0.30 x 0.20 x 0.05 mm^3	0.26 x 0.06 x 0.02 mm^3	0.15 x 0.12 x 0.03 mm^3	0.27 x 0.16 x 0.12 mm^3	0.28 x 0.24 x 0.17 mm^3	0.31 x 0.16 x 0.14 mm^3
Theta range for data collection	3.306 to 77.419°	4.181 to 77.338°.	3.788 to 67.055°.	3.431 to 77.294°.	2.944 to 76.682°.	2.828 to 77.433°.
Index ranges	-6<=h<=6, -20<=k<=21, -16<=l<=16	-13<=h<=12, -12<=k<=12, -27<=l<=24	-13<=h<=13, -10<=k<=4, -27<=l<=28	-11<=h<=11, -64<=k<=44, -12<=l<=10	-12<=h<=13, -9<=k<=7, -13<=l<=18	-12<=h<=13, -8<=k<=9, -19<=l<=17
Reflections collected	14940	31749	15522	23260	7091	7863
Independent reflections	5007	8877	5760	10786	3560	7863

	[R(int) = 0.0361]	[R(int) = 0.0488]	[R(int) = 0.0738]	[R(int) = 0.0384]	[R(int) = 0.0384]	[R(int) = 0.0708]
Completeness to theta = 67.684°	100.0 %	100.0 %	99.4 %	95.3 %	97.9 %	98.4 %
Absorption correction	Semi-empirical from equivalents	Gaussian	Semi-empirical from equivalents	Gaussian	Semi-empirical from equivalents	Semi-empirical from equivalents
Max. / min. transmission	1.00000 / 0.85477	1.000 / 0.632	1.00000 / 0.52137	1.000 / 0.462	1.00000 / 0.60966	1.00000 / 0.78661
Data / restraints / parameters	5007 / 243 / 424	8877 / 1 / 567	5760 / 1 / 566	10786 / 1 / 1120	3560 / 1 / 304	7863 / 1 / 313
Goodness-of-fit on F^2	1.033	1.072	1.074	1.052	1.056	1.100
Final R indices [I>2sigma(I)]	R1 = 0.0339, wR2 = 0.0836	R1 = 0.0392, wR2 = 0.0990	R1 = 0.0800, wR2 = 0.2265	R1 = 0.0461, wR2 = 0.1203	R1 = 0.0466, wR2 = 0.1239	R1 = 0.0659, wR2 = 0.1891
R indices (all data)	R1 = 0.0352, wR2 = 0.0847	R1 = 0.0428, wR2 = 0.1012	R1 = 0.1015, wR2 = 0.2489	R1 = 0.0480, wR2 = 0.1220	R1 = 0.0487, wR2 = 0.1258	R1 = 0.0726, wR2 = 0.1972
Flack parameter	0.09(8)	-0.12(7)	-0.2(3)	0.00(12)	-0.13(17)	0.2(3)
Largest diff. peak / hole	0.179 and -0.171 e.$Å^{-3}$	0.210 and -0.236 e.Å-3	0.662 / -0.418 e.$Å^{-3}$	0.413 / -0.287 e.$Å^{-3}$	0.314 / -0.276 e.$Å^{-3}$	0.252 and -0.291 e.$Å^{-3}$

Table S4: PXRD patterns of experimental screening

S/N	Coformer	PXRD Pattern
1	Amodiaquine 2HCL H20 (AQ)	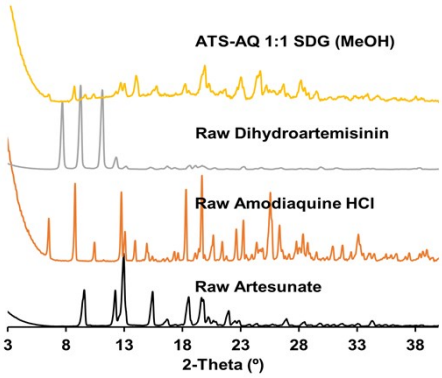
2	Pyrogallol (PG)	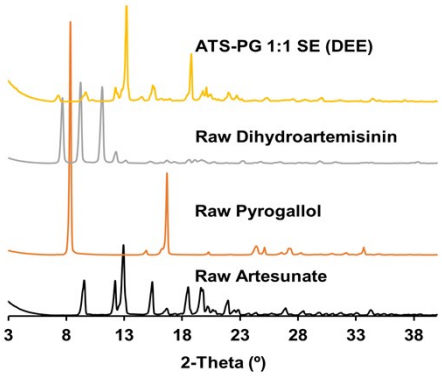
3	5-Flurocytosine (5-FC)	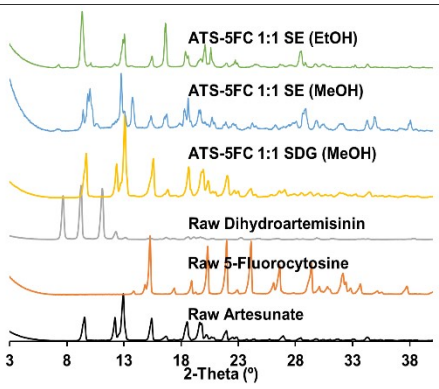
4	Ketoconazole (KCZ)	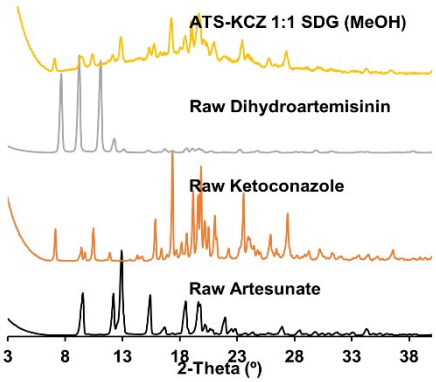
5	Urea (URE)	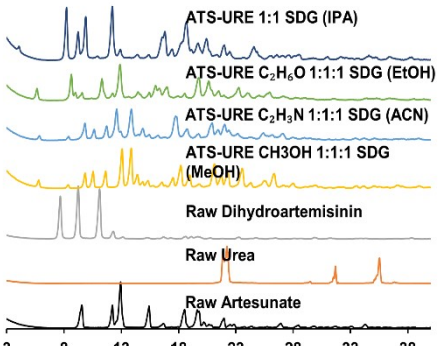

6	Riboflavin (RIB)	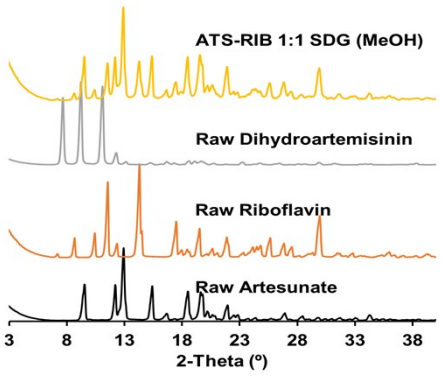
7	Cytosine (CYT)	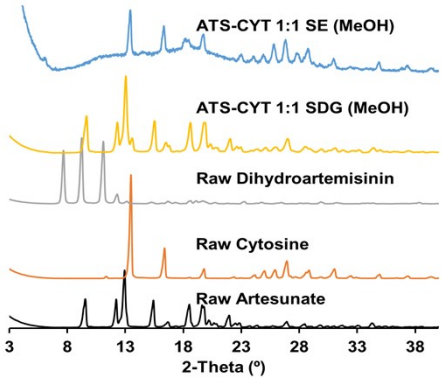
8	Clotrimazole (CTZ)	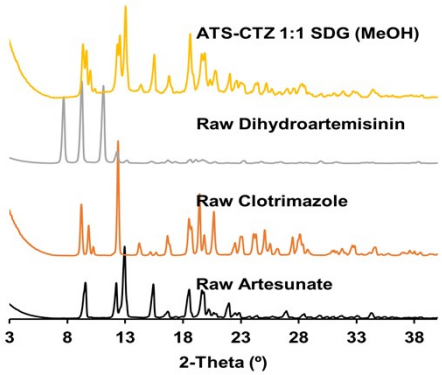
9	Allopurinol (ALO)	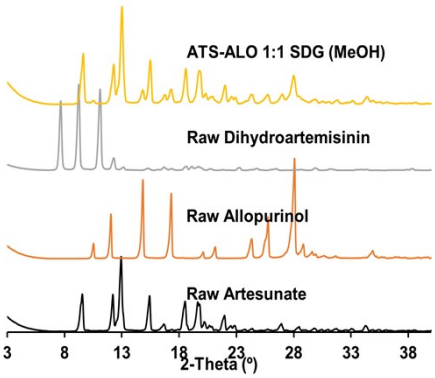
10	Climbazole (CLBZ)	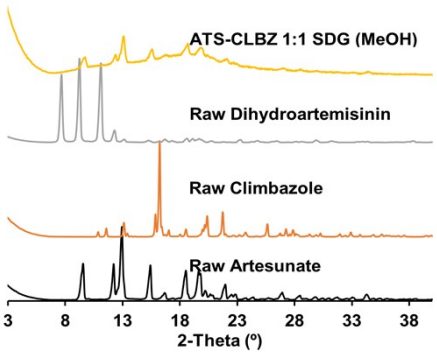

11	Pamoic acid (PMA)	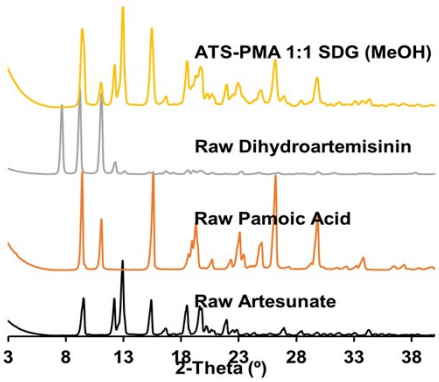
12	Fluconazole (FLZ)	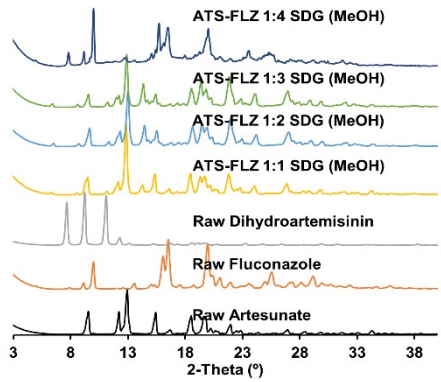
13	Niflumic acid (NFA)	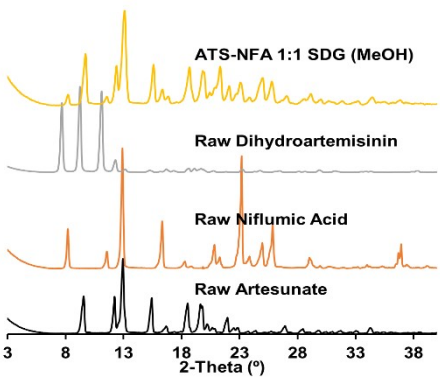
14	Carbamazepine (CBZ)	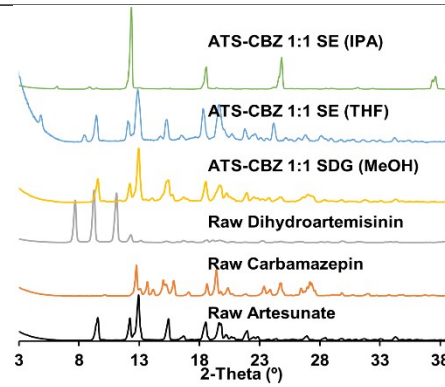
15	Flufenamic acid (FFA)	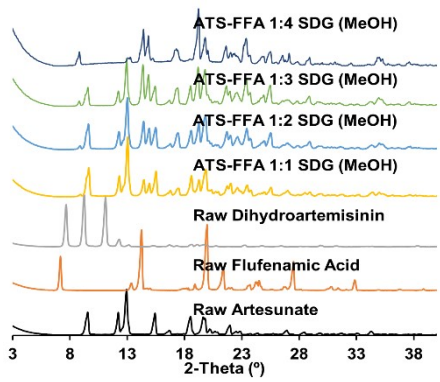

16	Quercetin (QUE)	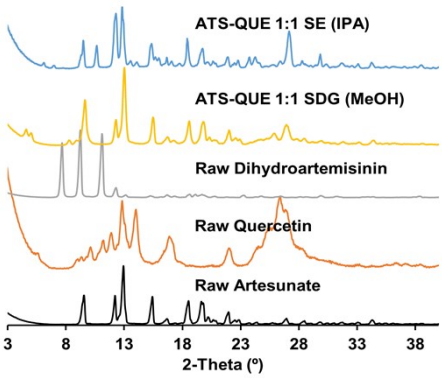
17	Luteolin (LUT)	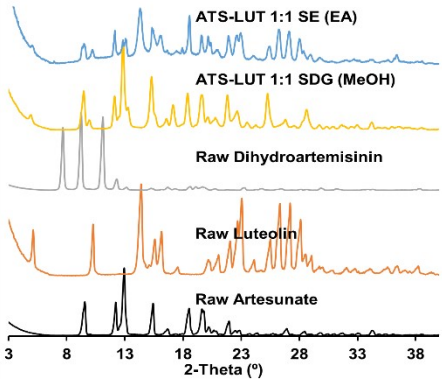
18	Ganciclovir (GCV)	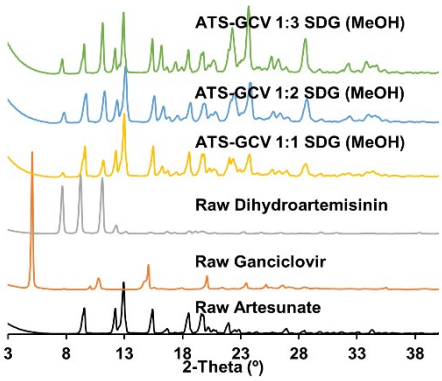
19	Pthalamide (PTA)	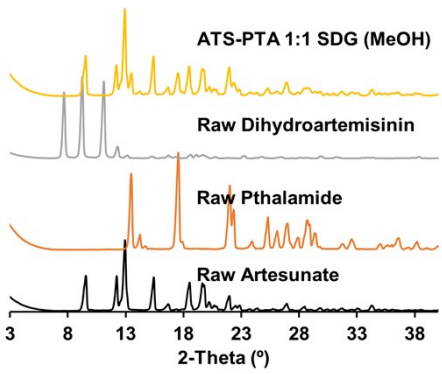
20	4-aminobenzoic acid (ABA)	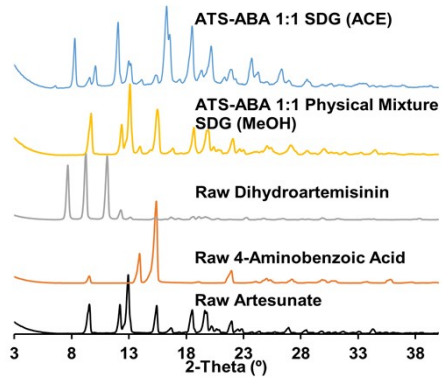

21	Etidronic acid (ETA)	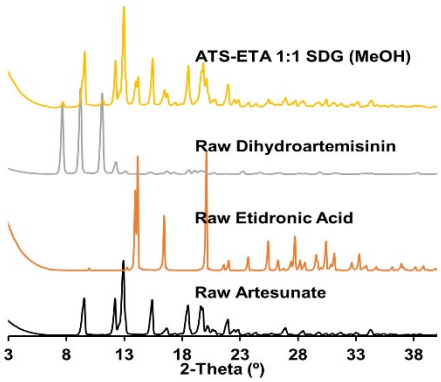
22	Ranitidine (RAN)	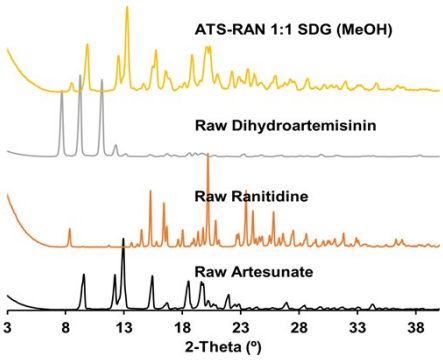
23	Albendazole (ABZ)	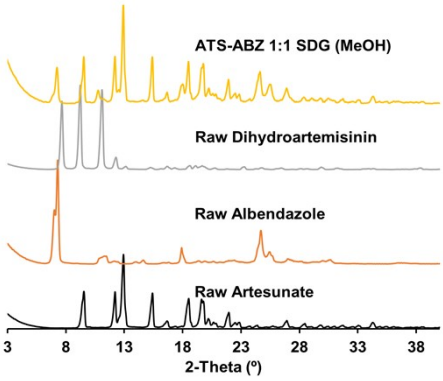
24	Itraconazole (ITZ)	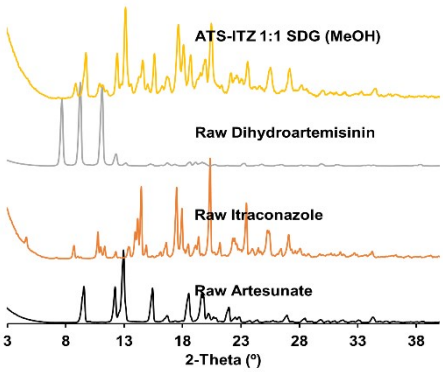

25	1,10-phenanthroline (PHEN)	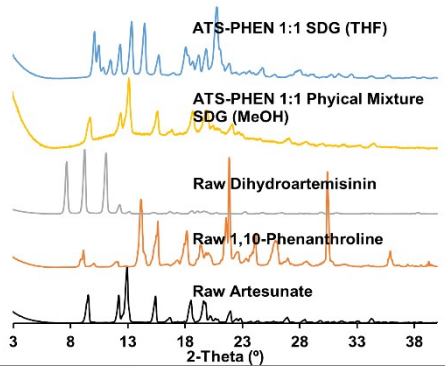
26	Resveratrol (RSV)	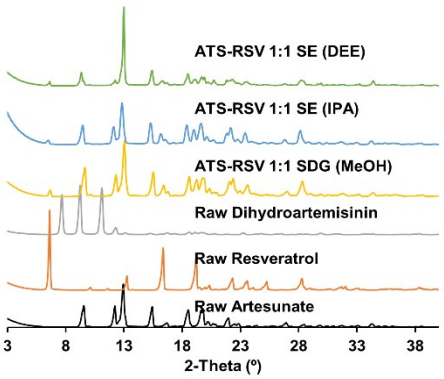
27	4-hydroxybenzohydrazide (HYB)	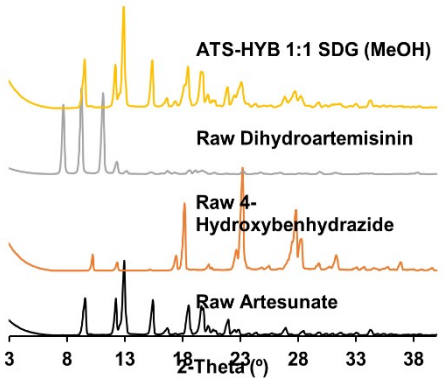
28	Biotin (BTN)	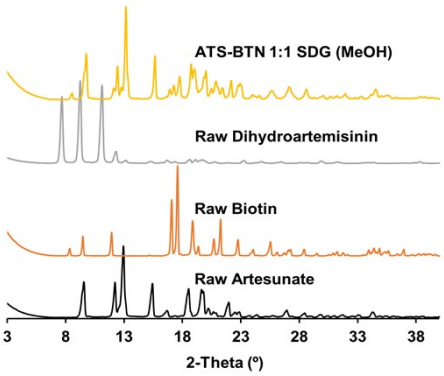
29	2-amino-5-methylbenzoic acid (AMBA)	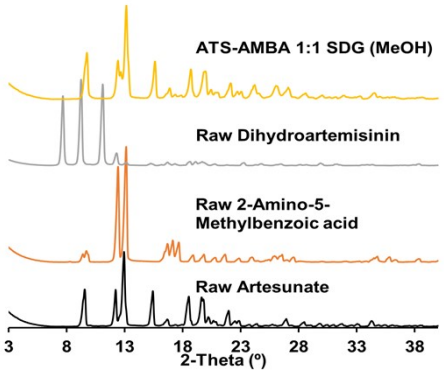

30	Curcumin (CUR)	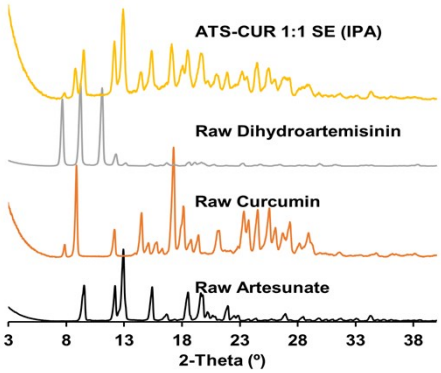
31	Voriconazole (VCZ)	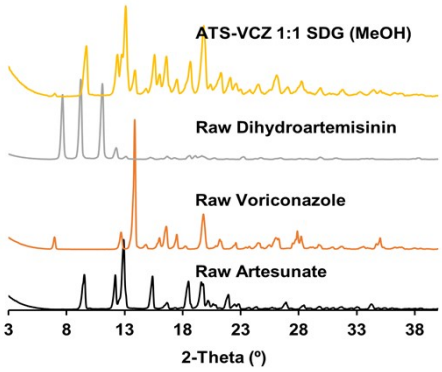
32	1,2-Di(pyridin-4-yl)ethane (DPE)	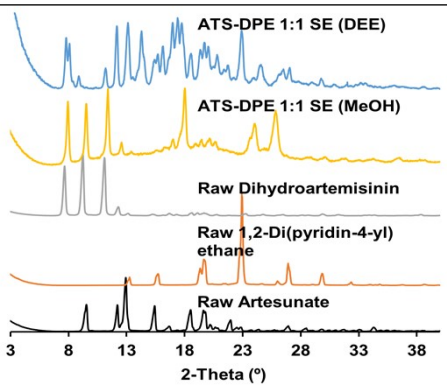
33	Acetone 1,3-dicarboxylic acid (ACDA)	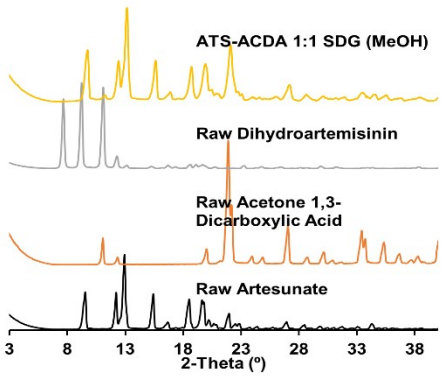
34	5-Fluorouracil (FLU)	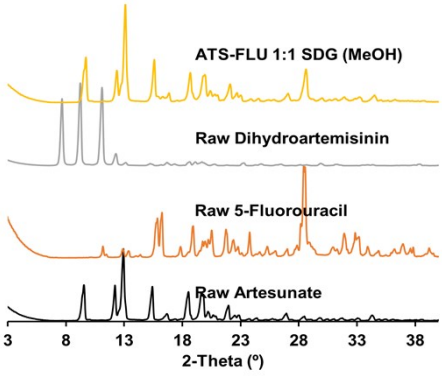

35	Oxalic acid (OA)	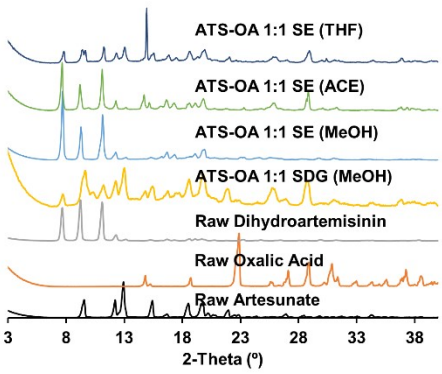
36	Paracetamol (PCM)	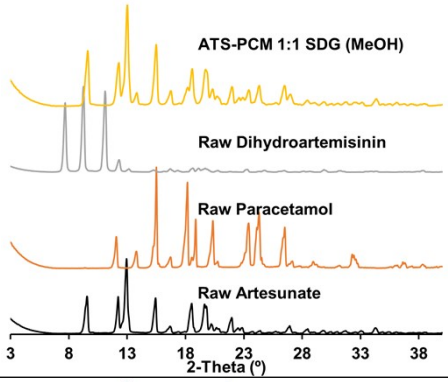
37	Piracetam (PIR)	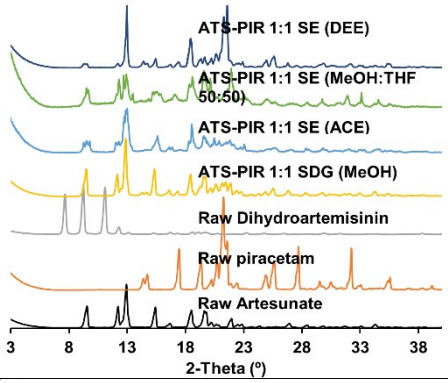
38	Apigenin (APG)	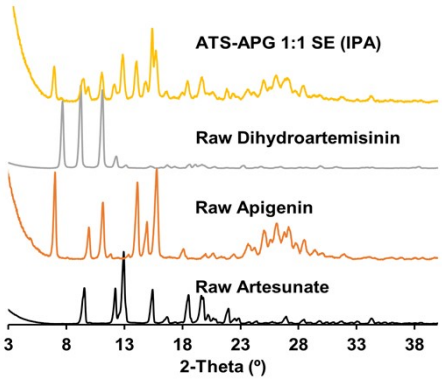
39	Isonicotinamide (INA)	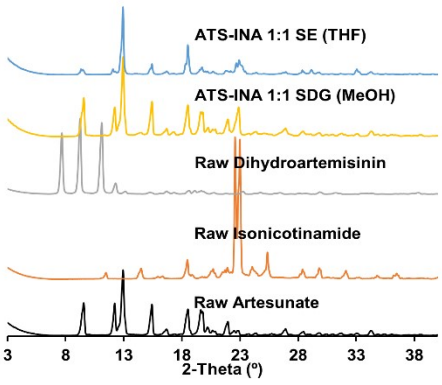

40	L-arginine (ARG)	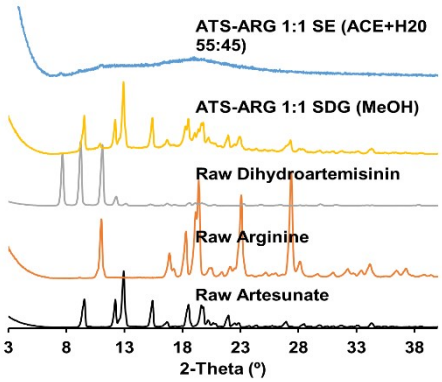
41	Xanthine (XAN)	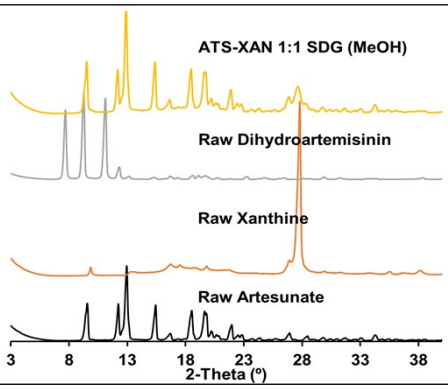
42	Hydrochlorothiazide (HCT)	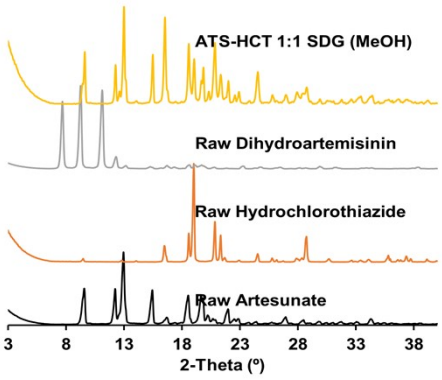
43	3-Aminopyridine (APR)	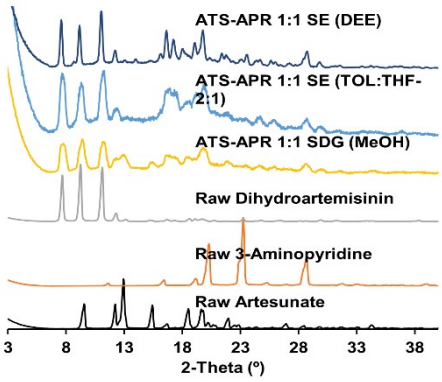
44	4-hydroxybenzoic acid (HYB)	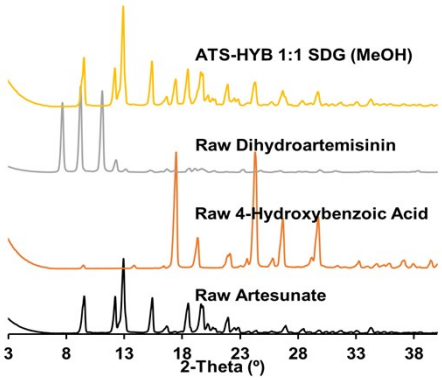

45	Saccharin (SAC)	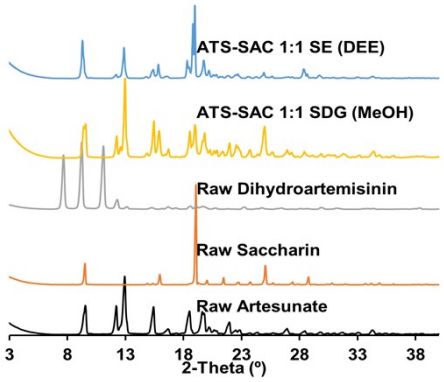
46	Hydroxyurea (HU)	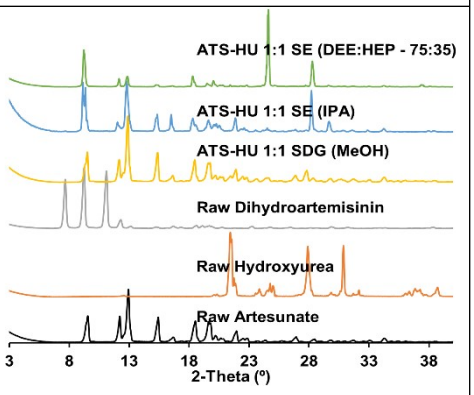
47	D-Glucoronic acid (D-GlcA)	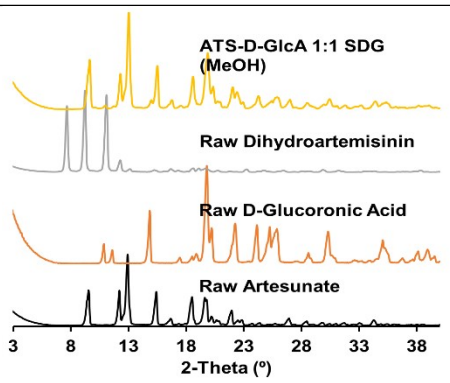
48	Hesperetin (HSP)	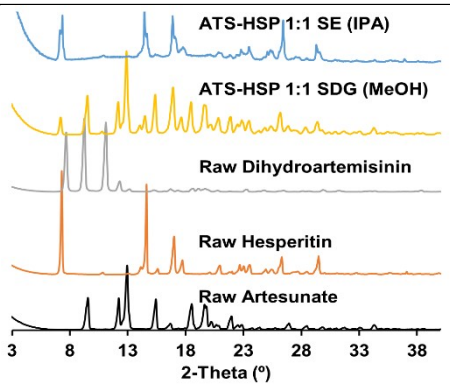
49	Daidzein (DAI)	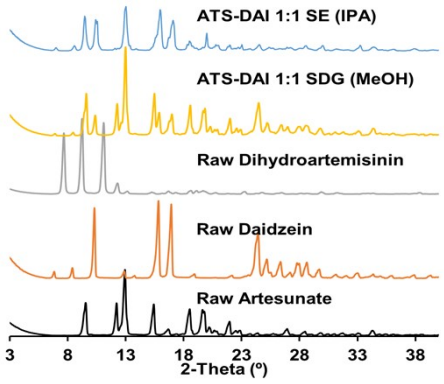

50	DL-Tryptophan (TRY)	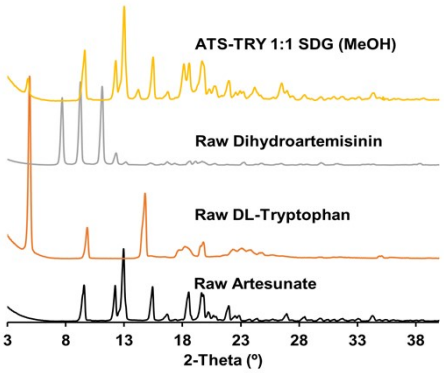
51	Praziquantel (PZQ)	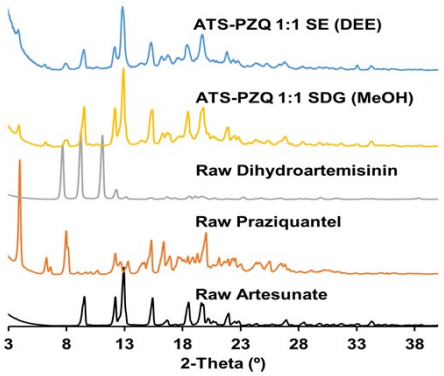
52	4,4-bipyridine (BPY)	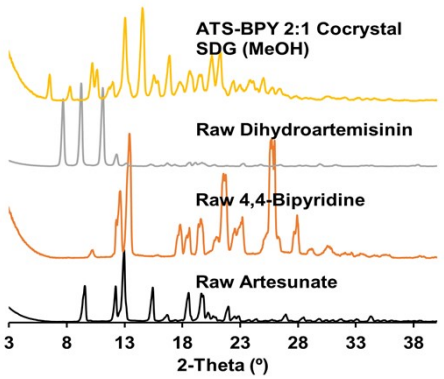
53	2-Ketoglutaric acid (KEA)	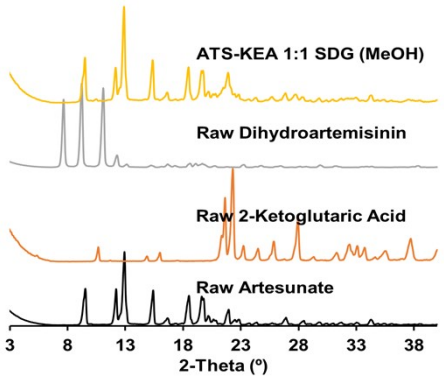
54	L-Tartaric acid (L-TA)	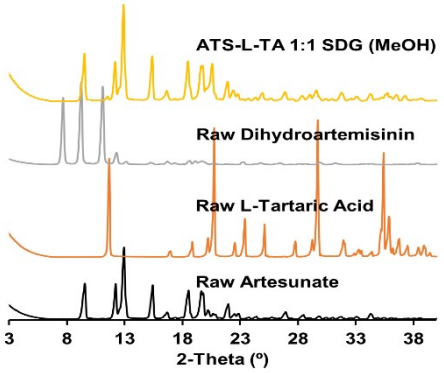

55	Nicotinamide (NIC)	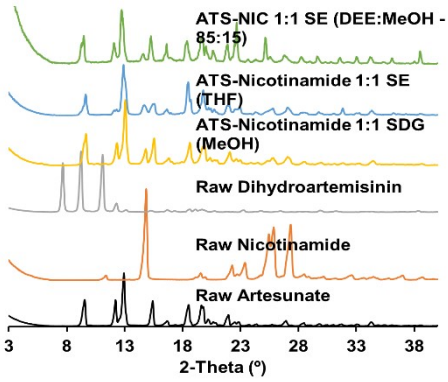
56	2,6- dihydrobenzoic acid (DHBA)	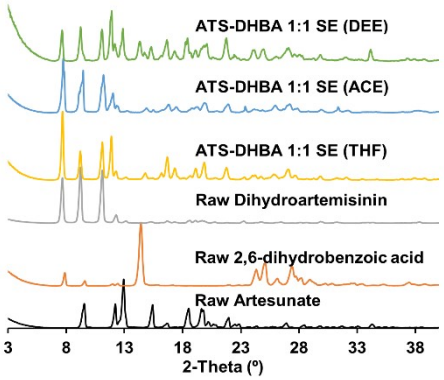
57	Tolfenamic acid (TFA)	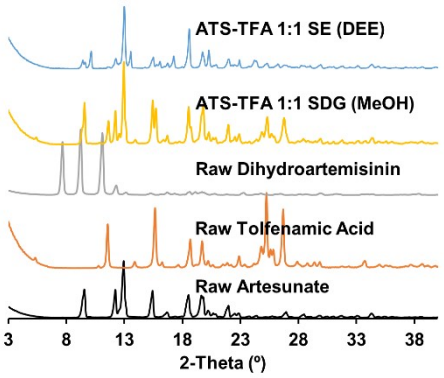
58	Isoniazid (INH)	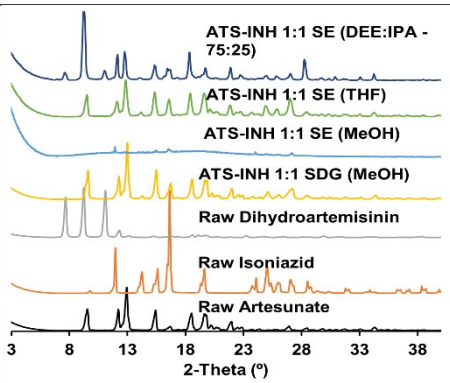
59	Malic acid (MA)	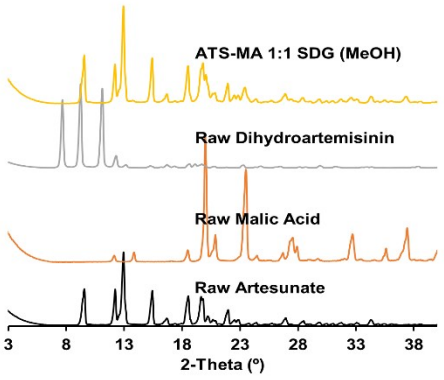

60	Glycine (GLY)	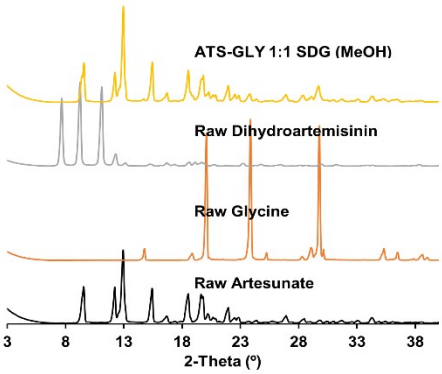
61	Xylitol (XLT)	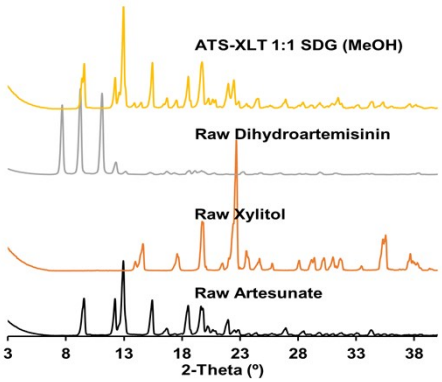
62	2-aminopyrazine (APY)	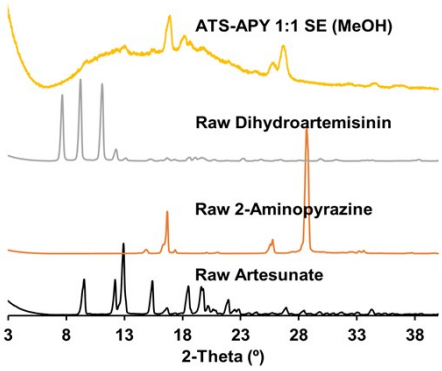
63	Cinnamic acid (Trans)	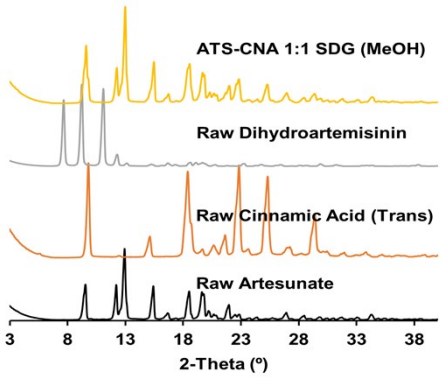
64	Pyrazinamide (PZA)	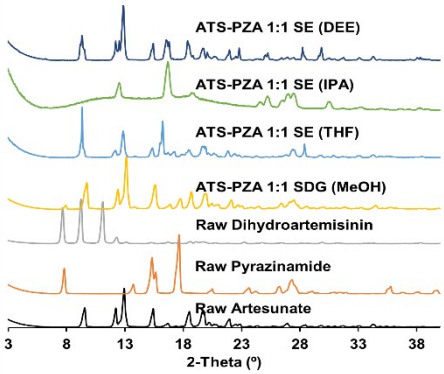

65	Levetiracetam (LEV)	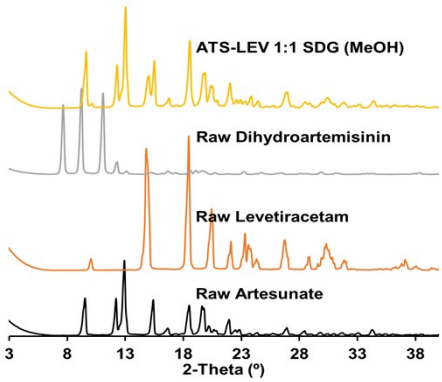
66	Muconic acid (MUCA)	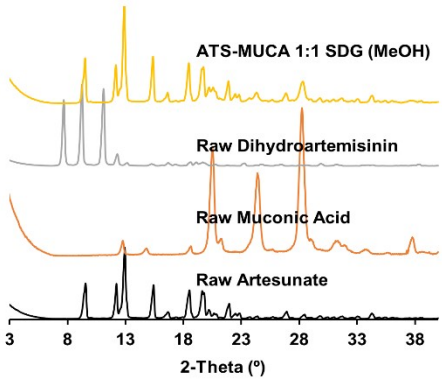
67	Hippuric acid (HIA)	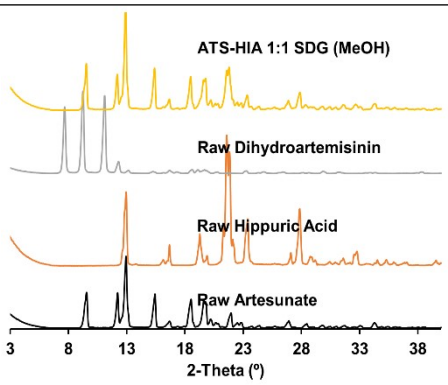
68	Imidazole (IMZ)	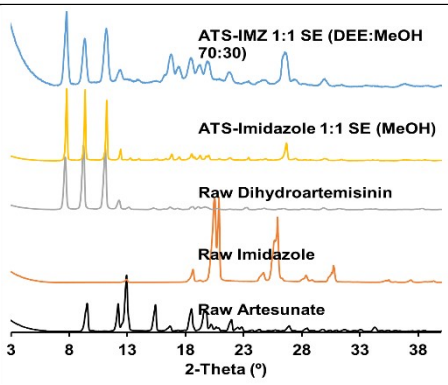
69	Aspartame (ASP-TM)	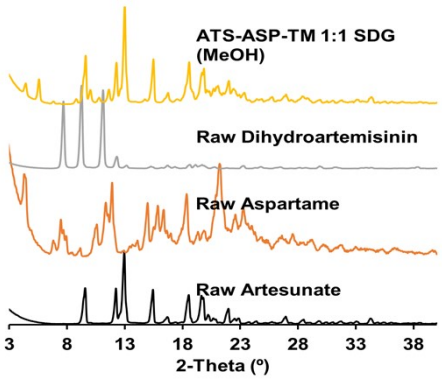

70	Lactose (LAC)	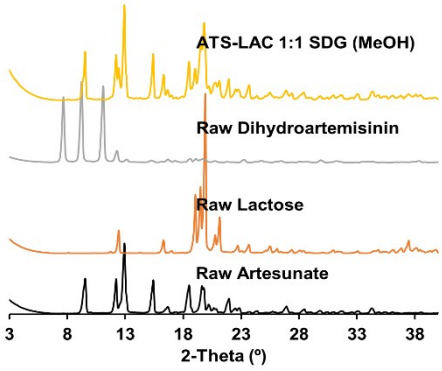
71	D-Phenylalanine (PHE)	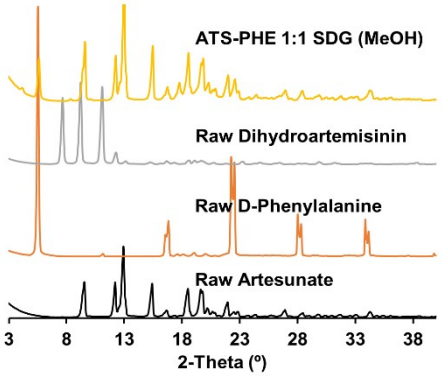
72	Naphthalene-2,6-dicarboxylic acid (NDA)	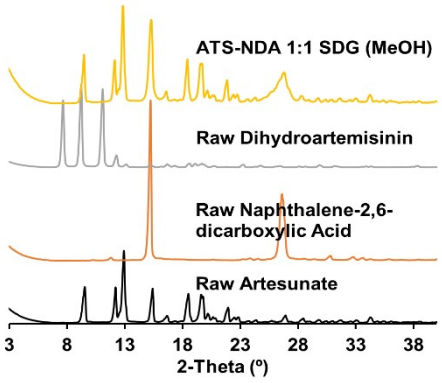
73	Indomethacin (IND)	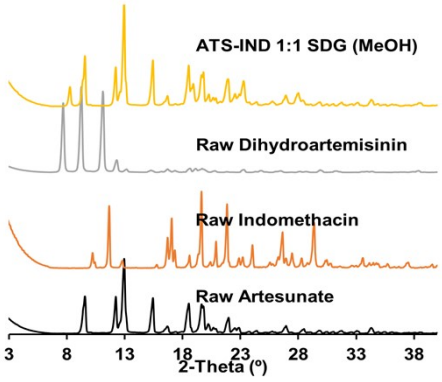
74	Glutaric acid (GLA)	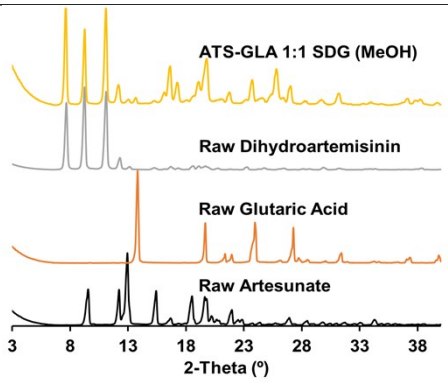

75	Chrysin (CSN)	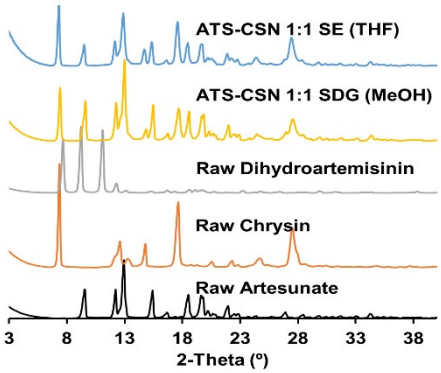
76	Citric acid (CA)	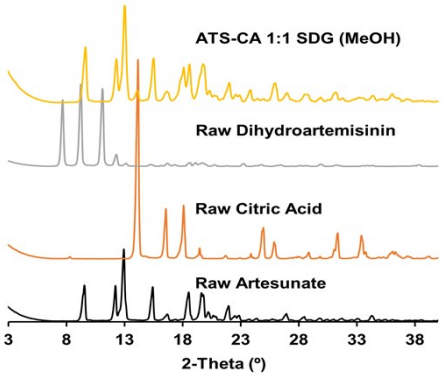
77	Maleic acid (MAA)	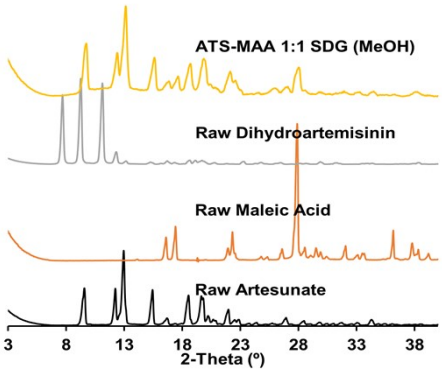
78	Itaconic acid (ITCA)	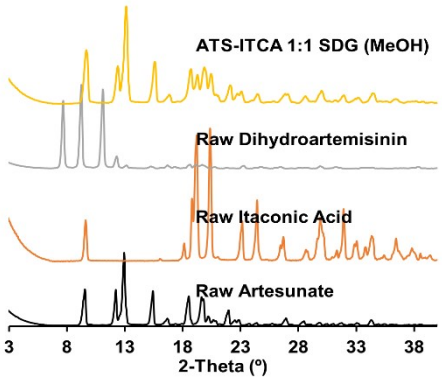
79	Ketoprofen (KTP)	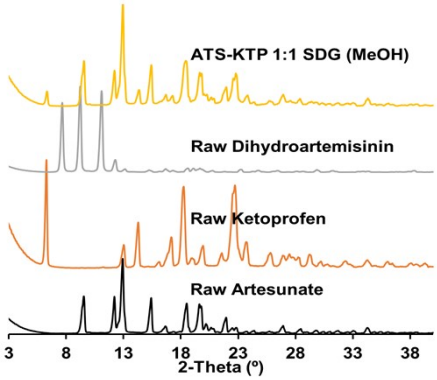

80	Nadolol (NAD)	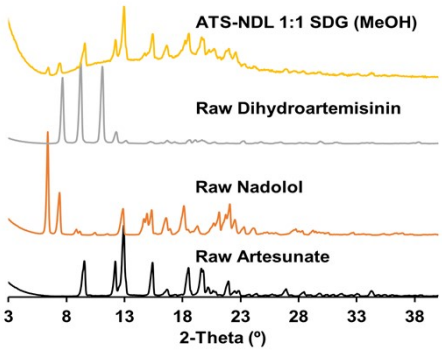
81	Citraconic acid (CTA)	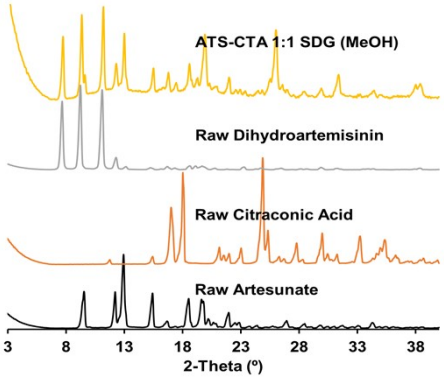
82	L-Glutamic (L-GLUA)	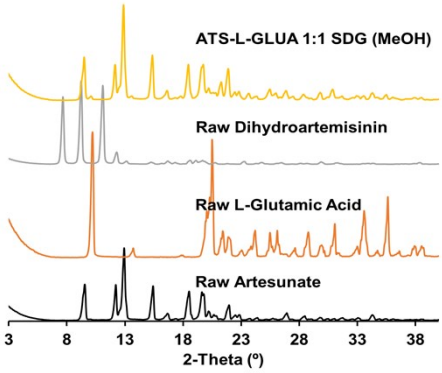
83	Cyclamic acid (CYA)	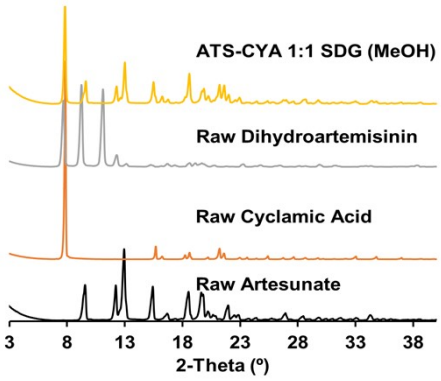
84	Fumaric Acid (FUMA)	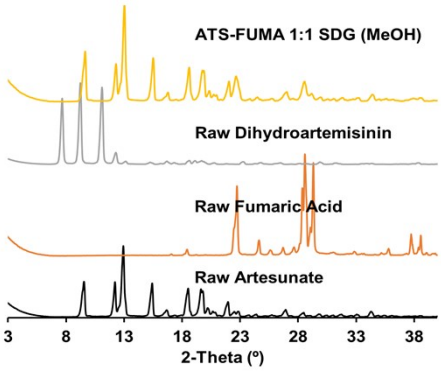

85	Acetophenone oxime (ACO)	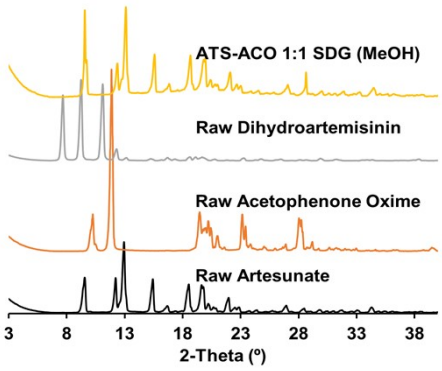
86	Sebacic acid (SEBA)	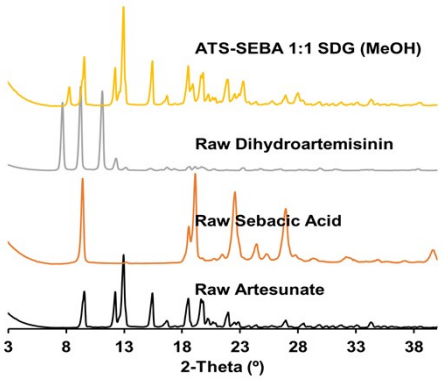
87	Mefenamic acid (MFA)	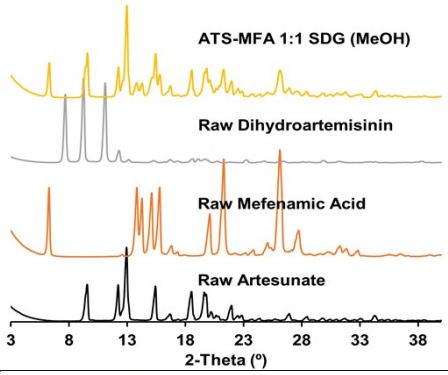
88	Salicyclic acid (SA)	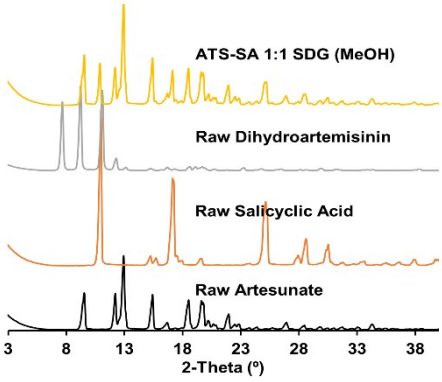

89	Artemisinin (ART)	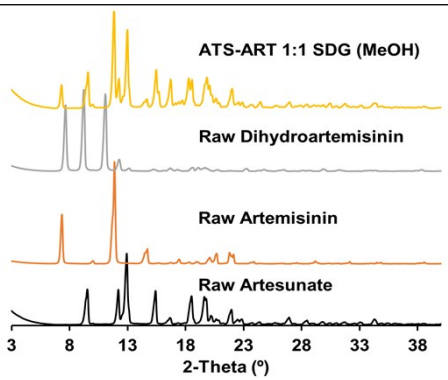
90	Succinic acid (SUA)	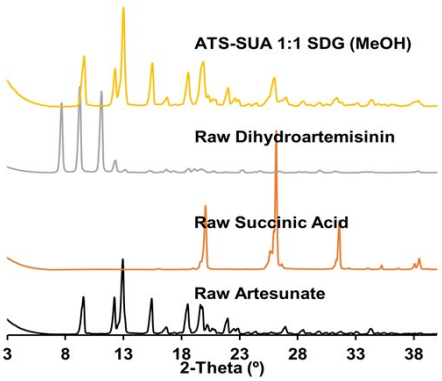
91	Mebendazole (MBZ)	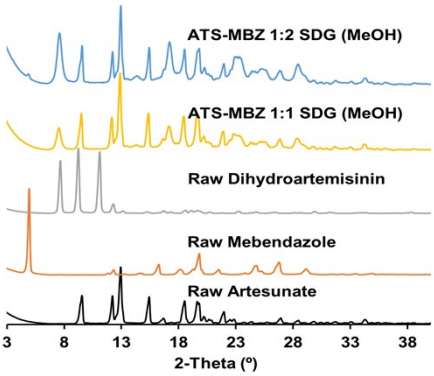
92	Folic acid (FA)	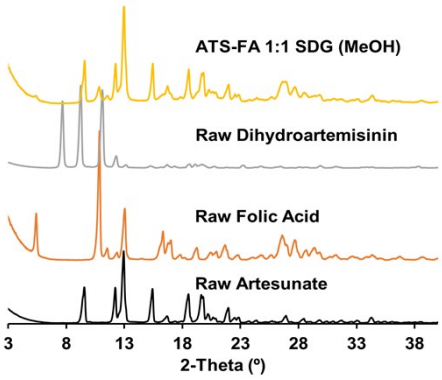
93	Benzoic acid (BZA)	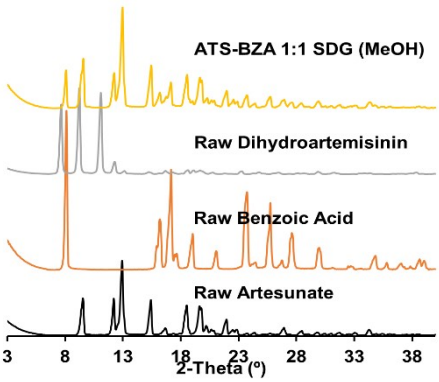

94	Pyrazine (PYR)	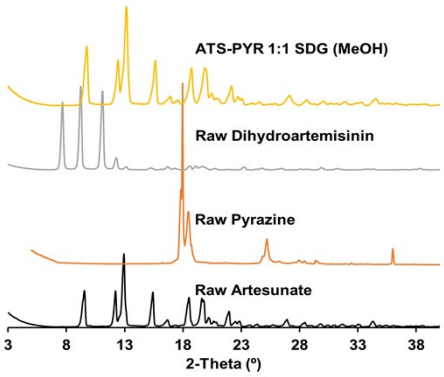
95	Pimelic acid (PIA)	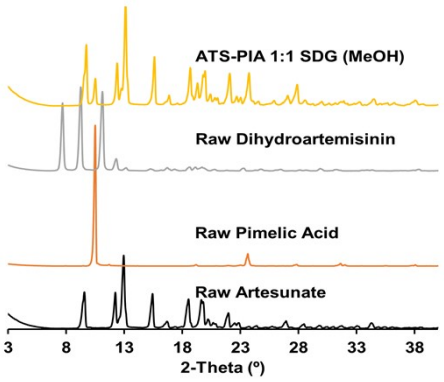
96	Caffeine (CAF)	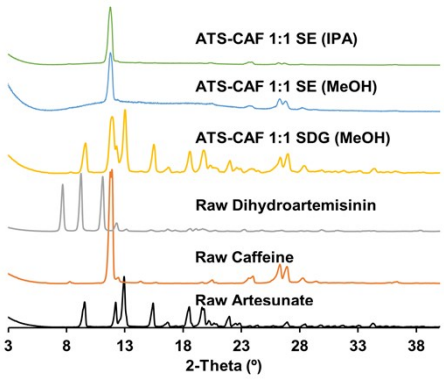
97	Azelaic acid (AZA)	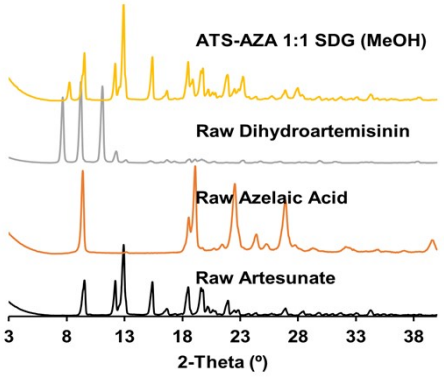
98	Ethylene Diamine Tetra Acetic Acid (EDTA)	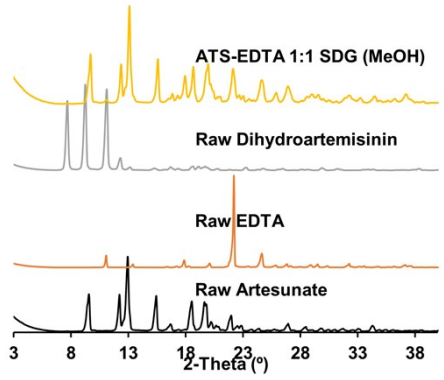

99	Aspirin (ASP)	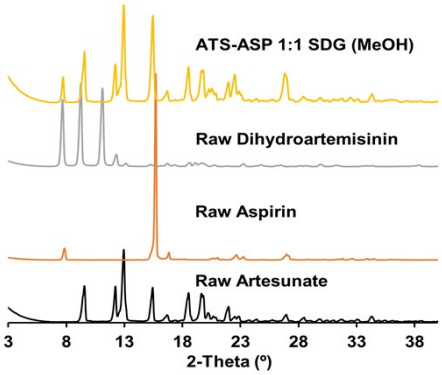
100	Terephthalic acid (TPA)	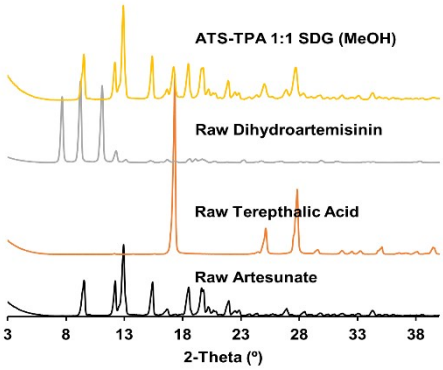
101	Phenazine (PHZ)	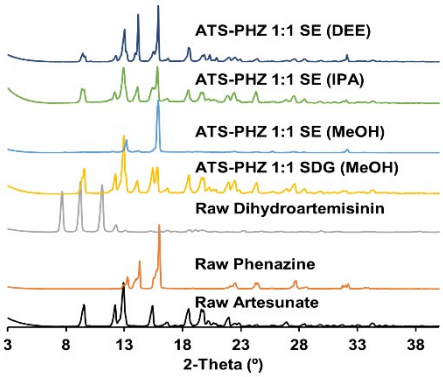
102	Piperazine (PIZ)	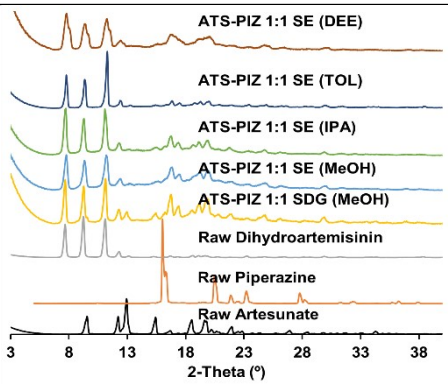
103	Isonicotinic acid (ISA)	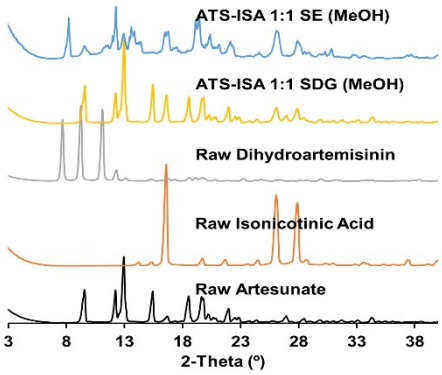

104	Suberic acid (SUBA)	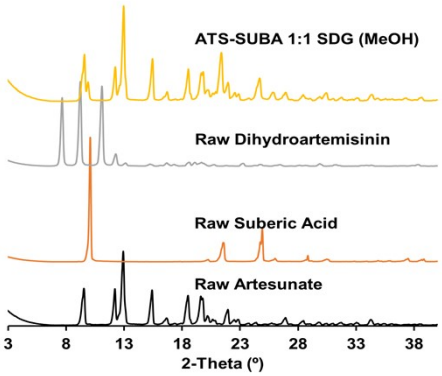
105	2-Picolinic Acid (2-PCA)	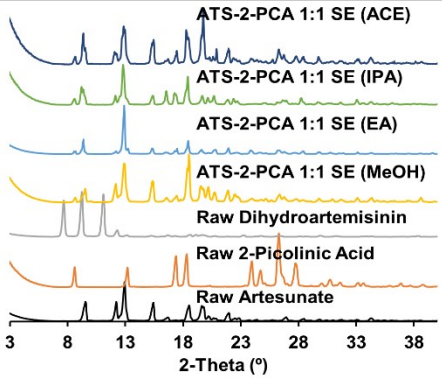
106	1,11-undecanedicarboxylic acid (UDCA)	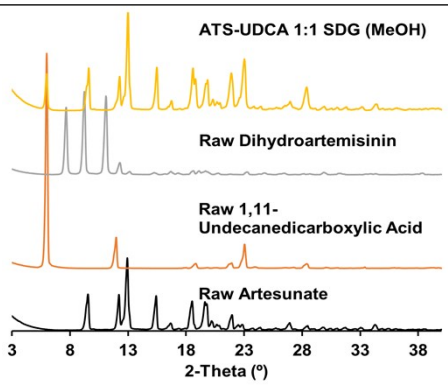
107	2-Aminopyrimidine (AMP)	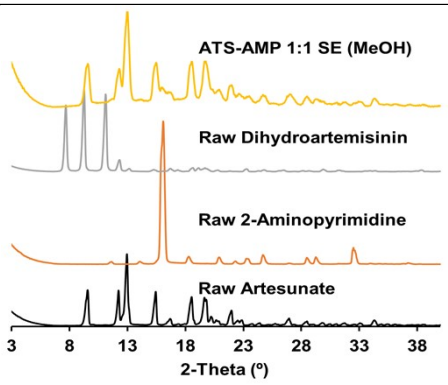
108	Adipic acid (ADA)	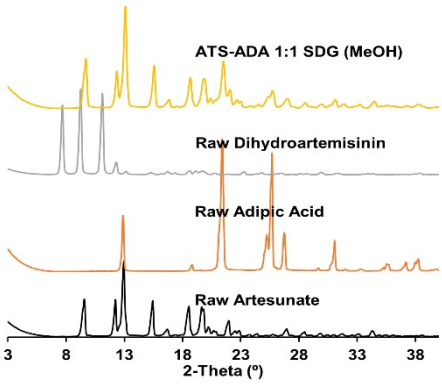

109	Nicotinic acid (NA)	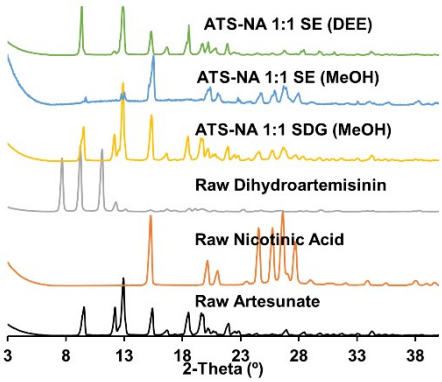
110	Methenamine (MEA)	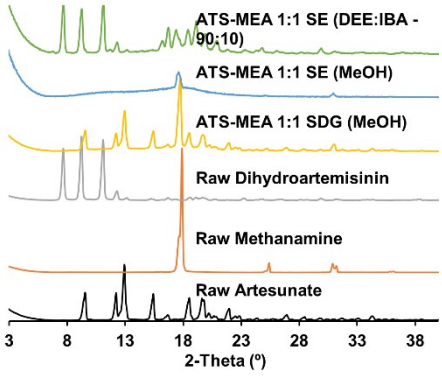
111	Theophylline (THP)	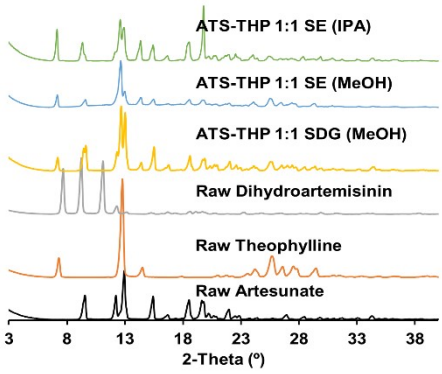
112	Cinchonidine (CNCD)	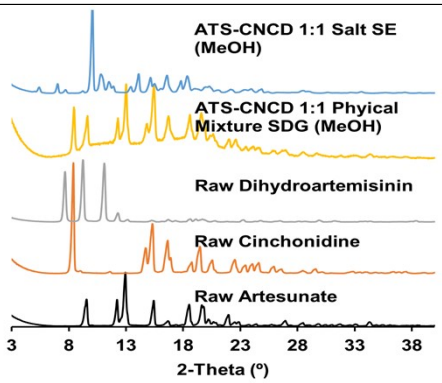
113	Theophylline-7-acetic acid (TAA)	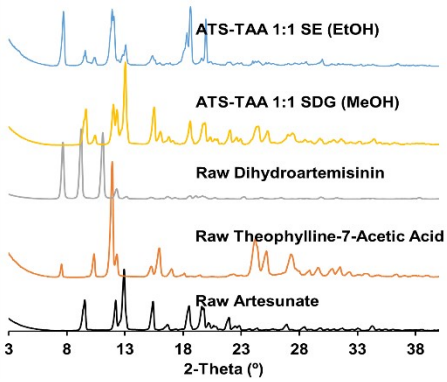

114	L-Proline (L-PRO)	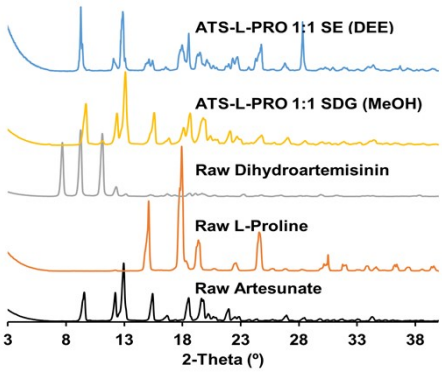
115	DL-Proline (DL-PRO)	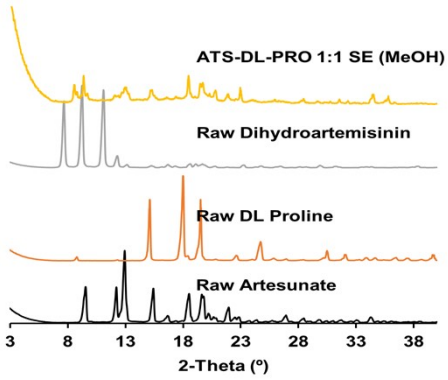
116	Ibuprofen (IBP)	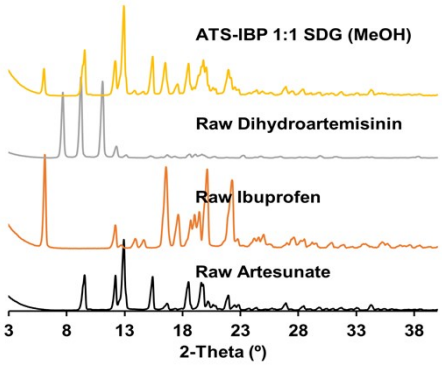
117	1,4-Diazabicyclo[2.2.2]octane (DABCO)	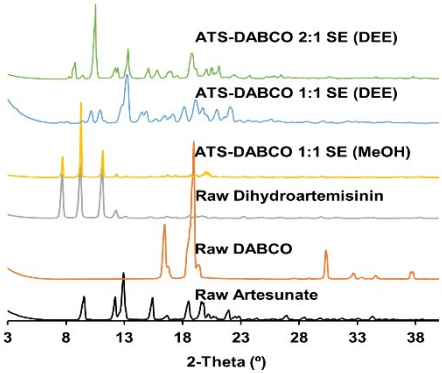

Table S5: ORTEP drawings of single-crystal X-ray structures of ATS cocrystals/salts

ATS cocrystals	ORTEP DRAWINGS
ATS-ABA	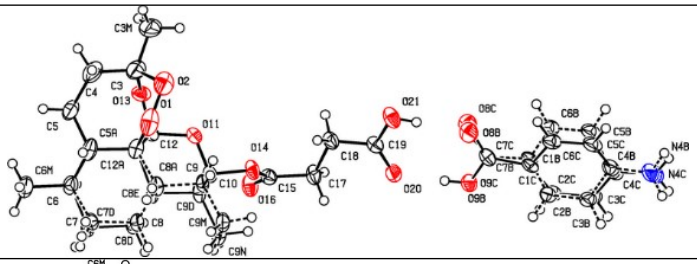
ATS^2-DABCO Form 1	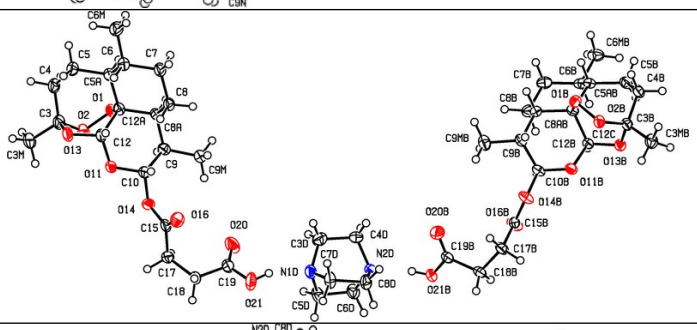
ATS^2-DABCO Form 2	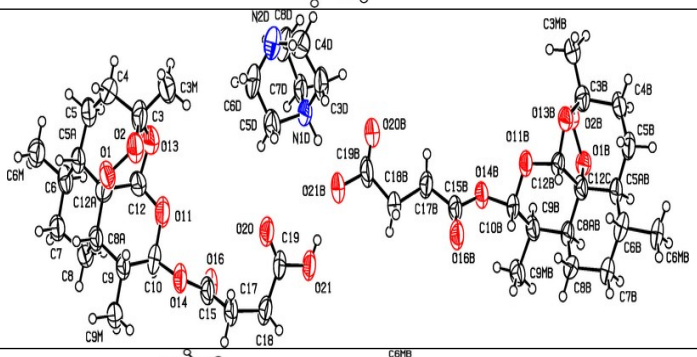
ATS-PHEN	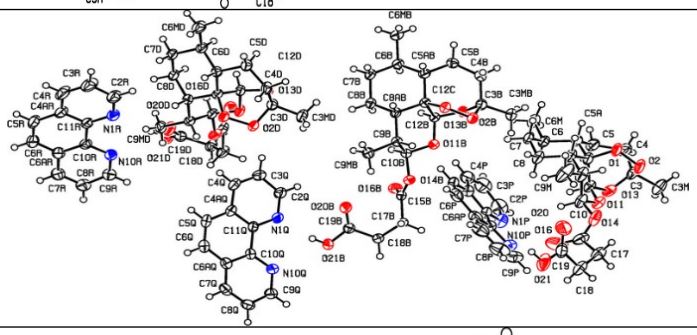
ATS-URE-CH_3OH	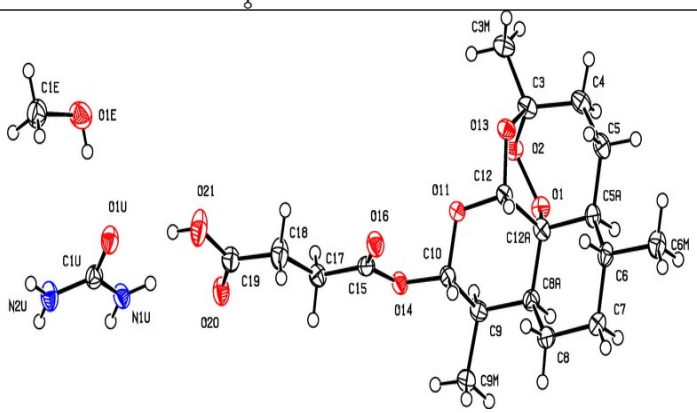

ATS-URE-C_2H_3N	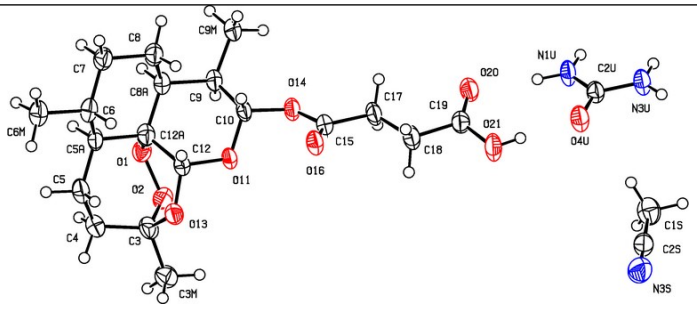

Table S6: FTIR spectra of ATS cocrystals/Salts

ATS cocrystal	FTIR spectra	Peak alterations
ATS-ABA	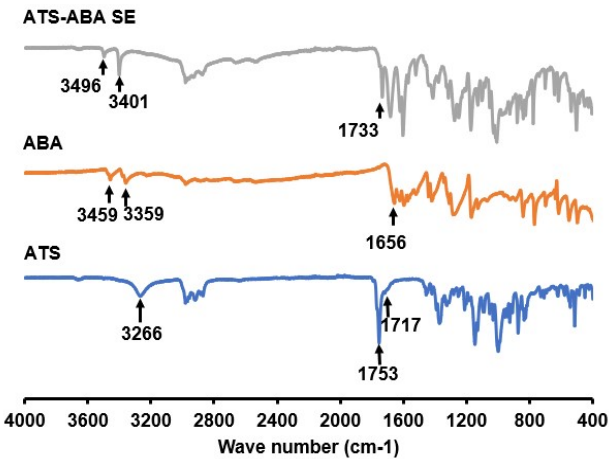	In the ATS spectra, the O-H stretching band at 3266 cm^{-1} was absent in the ATS-ABA sample due to intermolecular hydrogen bonding [1]. The carbonyl C=O stretching band, initially at 1753 cm^{-1} in the ATS, shifted to 1733 cm^{-1} and exhibited reduced intensity in the ATS-ABA. These shifts in the carbonyl peak positions could suggest the formation of intermolecular hydrogen bonds or alterations in the intermolecular arrangement, as corroborated by the SXRD results [2, 3]. In the coformer ABA, the N-H stretching vibrations initially observed at 3459 and 3359 cm^{-1} shifted to 3496 and 3401 cm^{-1}, respectively. This indicates that the N-H bands are still present in the IR spectra of ATS-ABA and that proton transfer has not occurred. Additionally, the carbonyl stretching band at 1656 cm^{-1} has shifted to 1682 cm^{-1} due to the formation of hydrogen bonding [2]. These observations suggest that ATS-ABA is a cocrystal, as no proton transfer has been observed.
ATS^2-DABCO Form 1	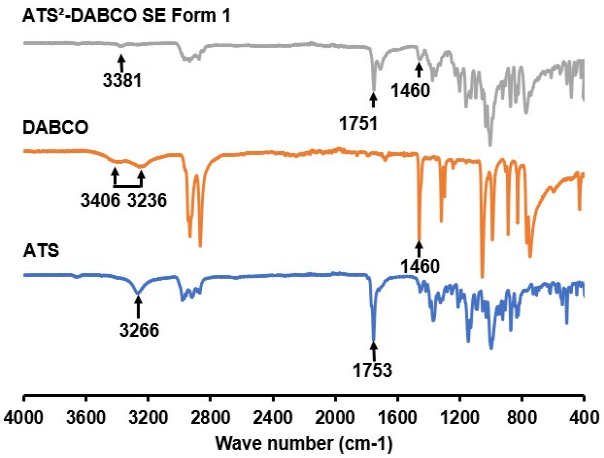	The O-H stretching band at 3266 cm^{-1} observed in ATS appeared to have been lost in ATS^2-DABCO Form 1 due to intermolecular hydrogen bonding [1]. Additionally, the carbonyl C=O stretching band at 1753 cm^{-1} in ATS shifted to 1751 cm^{-1} in ATS^2-DABCO Form 1 and exhibited significantly reduced intensity, likely due to intermolecular hydrogen bonding [2, 3]. The broad O-H stretching vibrations between 3406 and 3236 cm^{-1} in the DABCO range indicate the presence of water, a finding validated by the DSC results, this stretching appeared to have shifted to 3381 cm^{-1} with significantly reduced intensity in ATS^2-DABCO Form 1 due to intermolecular hydrogen bonding [2, 3].

		Additionally, the sharp C-N stretching band in DABCO, originally at 1460 cm^{-1}, was maintained but exhibited significantly reduced intensity in ATS²-DABCO Form 1. This reduction in intensity could indicate the formation of intermolecular hydrogen bonds. Based on these observations, ATS²-DABCO Form 1 can be identified as a cocrystal.
ATS²-DABCO Form 2	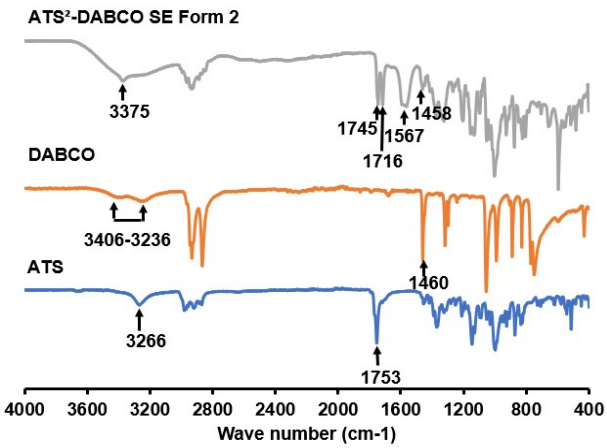	In ATS²-DABCO Form 2, the O-H stretching band of ATS at 3266 cm^{-1} appears to have merged with the broad band of DABCO at 3375 cm^{-1}, potentially due to intermolecular hydrogen bonding with DABCO. Furthermore, the carbonyl C=O stretching band, initially observed at 1753 cm^{-1}, appears to have split and shifted to 1745 and 1716 cm^{-1}, exhibiting reduced intensity. This change is likely due to different chemical environments and interactions for the carbonyl groups as a result of intermolecular hydrogen bondin [2, 3] or partial deprototonation. The broad O-H stretching vibrations between 3406 and 3236 cm^{-1} in the DABCO range indicate the presence of water, a finding validated by the DSC results. This band has shifted into a broader band at 3375 cm^{-1} with increased intensity in the ATS²-DABCO Form 2. The sharp C-N stretching band at 1460 cm^{-1} shifted to 1458 cm^{-1} in ATS²-DABCO Form 2, with significantly reduced intensity, possibly due to intermolecular hydrogen bonding. Additionally, a new peak at 1567 cm^{-1} was observed, which could be attributed to the presence of a carboxylate ion, suggesting deprotonation [1]. These observations suggest that a salt has been formed.
ATS²-DPE		The O-H stretching band in DPE was lost in ATS²-DPE possibly due to intermolecular hydrogen bonding [1]. The 1753 cm^{-1} carbonyl C=O stretching in ATS shifted to 1750 cm^{-1} in ATS²-DPE with reduced intensity indicating a

	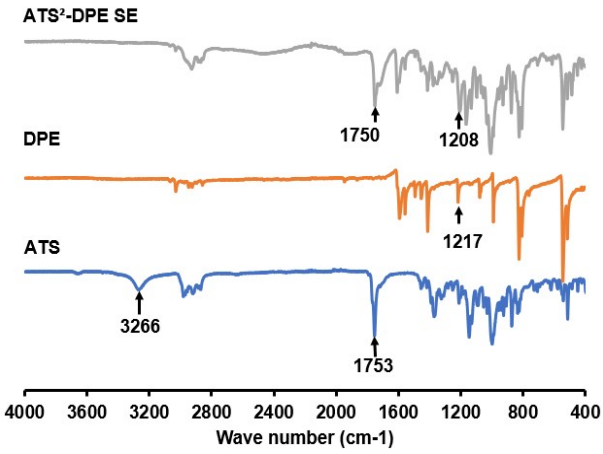	potential intermolecular hydrogen bonding. The C-N stretching vibration at 1217 cm^{-1} in DPE appears to have shifted to 1208 cm^{-1} in ATS²-DPE, with increased intensity, suggesting possible intermolecular hydrogen bonding. These results indicate the formation of a cocrystal, as there is no evidence of protonation or deprotonation.
ATS-PHEN	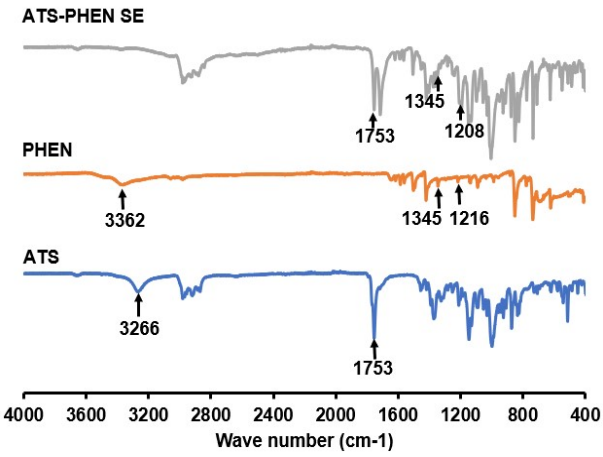	The O-H stretching band at 3266 cm^{-1} in ATS was lost in ATS-PHEN due to intermolecular hydrogen bonding [1]. The carbonyl C=O stretching band at 1753 cm^{-1} maintained its position but showed a reduction in intensity. The peak at 3362 cm^{-1} in PHEN may be attributed to impurities, as PHEN itself does not exhibit N-H or O-H stretching vibrations. The C-N stretching vibrations observed at 1345 cm^{-1} and 1216 cm^{-1} in PHEN were maintained at 1345 cm^{-1} and 1208 cm^{-1} in ATS-PHEN, respectively, with a reduction in intensity. This change is likely due to the formation of intermolecular hydrogen bonding with no proton transfer. This shows that a cocrystal is formed.
ATS-URE	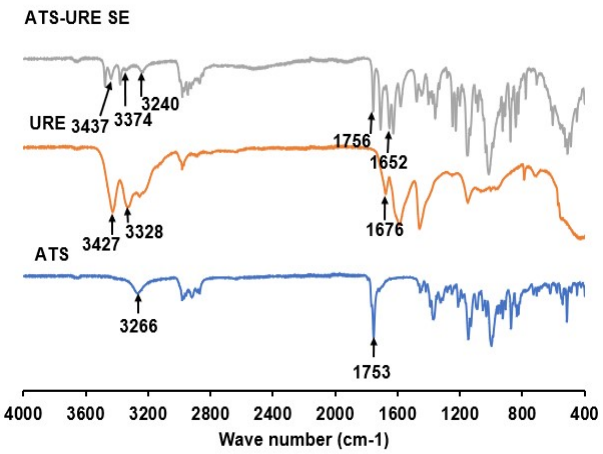	The O-H stretching band in ATS has shifted from 3266 cm^{-1} to 3240 cm^{-1} in ATS-URE, with a reduction in intensity. The carbonyl C=O stretching band at 1753 cm^{-1} has shifted to 1556 cm^{-1} due to the formation of intermolecular hydrogen bonding between ATS and URE [2, 3]. The dual N-H stretching bands in URE, originally at 3328 cm^{-1} and 3427 cm^{-1}, have shifted to 3374 cm^{-1} and 3437 cm^{-1}, respectively, both with reduced intensity. The carbonyl (C=O) group band at 1676 cm^{-1} has either been lost or shifted to 1627 cm^{-1}. As N-H stretching bands are was still

		maintained, it suggested that no proton transfer has taken place suggesting that a cocrystal has been formed [2].
ATS-URE-CH_3OH	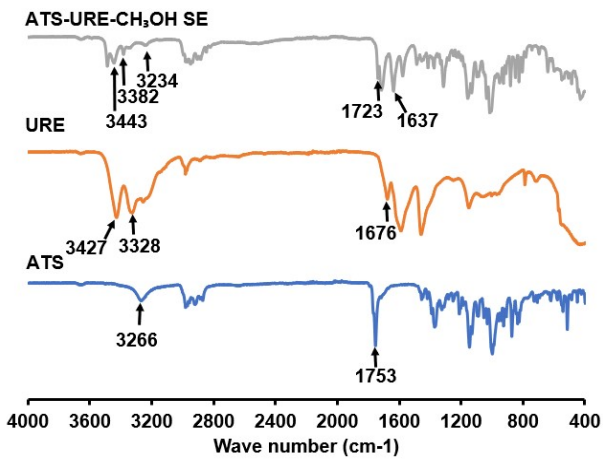	The O-H stretching band in ATS has shifted from 3266 cm^{-1} to 3234 cm^{-1} in ATS-URE-CH_3OH with a reduction in intensity. The ATS carbonyl C=O stretching band at 1753 cm^{-1} has shifted to 1723 cm^{-1} in ATS-URE-CH_3OH. These changes could suggest the formation of intermolecular hydrogen bonding [2, 3]. The dual N-H stretching bands in URE, originally at 3328 cm^{-1} and 3427 cm^{-1}, have shifted to 3382 cm^{-1} and 3443 cm^{-1}, respectively, both with reduced intensity. The carbonyl (C=O) group band at 1676 cm^{-1} has shifted to 1637 cm^{-1}. As the N-H stretching bands were still maintained, this suggests that no proton transfer has taken place, indicating that a cocrystal has been formed [2].
ATS-URE-C_2H_6O	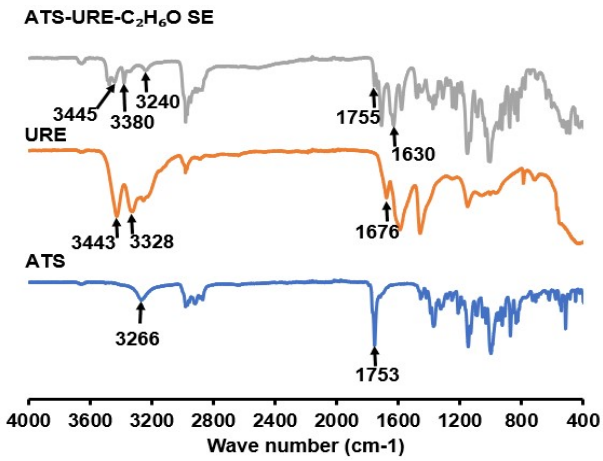	The O-H stretching band in ATS has shifted from 3266 cm^{-1} to 3240 cm^{-1} in ATS-URE- C_2H_6O with a reduction in intensity. The ATS carbonyl C=O stretching band at 1753 cm^{-1} has shifted to 1755 cm^{-1} in ATS-URE-C_2H_6O with significantly reduced intensity. These changes could suggest the formation of intermolecular hydrogen bonding between ATS, URE, and C_2H_6O [2, 3]. The dual N-H stretching bands in URE, originally at 3328 cm^{-1} and 3427 cm^{-1}, have shifted to 3380 cm^{-1} and 3445 cm^{-1}, respectively, both with reduced intensity. The carbonyl (C=O) group band at 1676 cm^{-1} has shifted to 1630 cm^{-1}. As the N-H stretching bands were still maintained and no significant change in the positions of the C=O stretching, this suggests that no proton transfer has taken place, indicating that a cocrystal has been formed [2].
ATS-URE-C_2H_3N		The O-H stretching band in ATS has shifted from 3266 cm^{-1} to 3233 cm^{-1} in ATS-URE- C_2H_3N with a reduction in intensity. The ATS carbonyl C=O stretching band at 1753 cm^{-1} has shifted to

	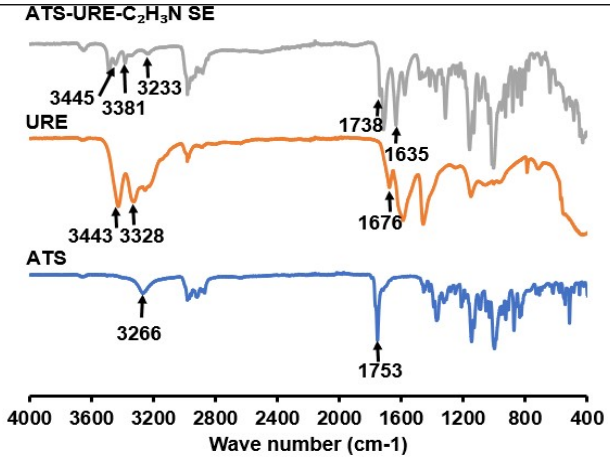	1738 cm^{-1} in ATS-URE-C_2H_3N with significantly reduced intensity. These changes could suggest the formation of intermolecular hydrogen bonding between ATS, URE, and C_2H_3N [2, 3]. The dual N-H stretching bands in URE, originally at 3328 cm^{-1} and 3427 cm^{-1}, have shifted to 3381 cm^{-1} and 3445 cm^{-1}, respectively, both with reduced intensity. The carbonyl (C=O) group band at 1676 cm^{-1} has shifted to 1635 cm^{-1}. As the N-H stretching bands were still maintained and no significant change in the positions of the C=O stretching, this suggests that no proton transfer has taken place, indicating that a cocrystal has been formed [2].

Table S7: Calibration model of ATS using HPLC (methanol was employed to prepare all the solutions measured). The concentration units are in µg/mL; Cr: theoretical concentration of the validation sample and Cm: measured concentration of the validation sample.

Calibration Curve range (µg/mL)	Concentration points (µg/mL)	Calibration graph	Validation samples		
			C_r (µg/mL)	C_m (µg/mL)	$\frac{C_m - C_r}{C_r} x100$
5 - 500	5,10, 20, 50, 100, 150, 250, 500	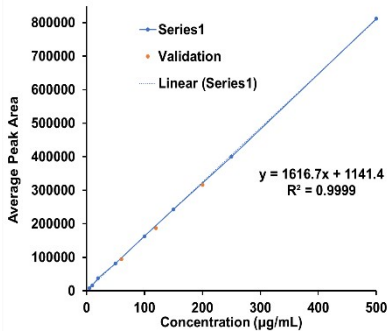	60	62.31	3.84
			120	118.90	0.92
			200	199.14	0.43

Table S8: Calibration model of DHA using HPLC (methanol was employed to prepare all the solutions measured). The concentration units are in µg/mL; Cr: theoretical concentration of the validation sample and Cm: measured concentration of the validation sample.

Calibration Curve range (µg/mL)	Concentration points (µg/mL)	Calibration graph	Validation samples		
			C_r (µg/mL)	C_m (µg/mL)	$\frac{C_m - C_r}{C_r} x100$
1.875 - 150	1.875, 3.75, 7.5, 15, 30, 90, 150	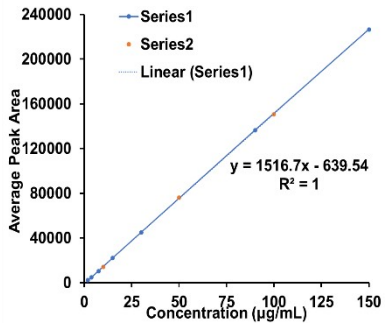	10	9.83	1.74
			50	50.52	1.04
			100	99.8	0.20

Table S9: Single Cocrystal images and Morphology prediction

Cocrystal sample	Single cocrystal image	Morphology prediction
ATS-ABA		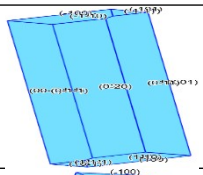
ATS^2-DABCO Form 1		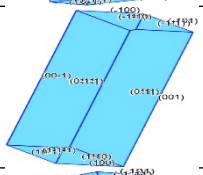
ATS^2-DABCO Form 2		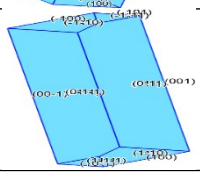
ATS^2-DPE	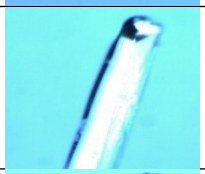	
ATS-PHEN	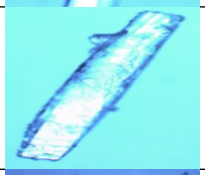	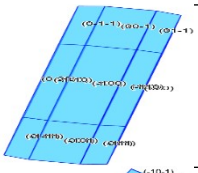
ATS-URE	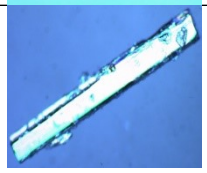	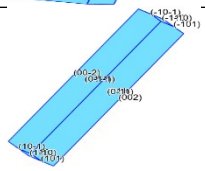
ATS-URE- CH_3OH	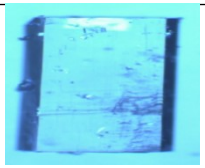	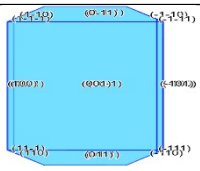
ATS-URE- C_2H_6O	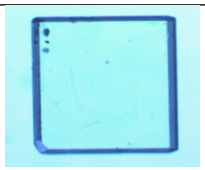	The structure was not determined due to poor diffraction quality.
ATS-URE- C_2H_3N	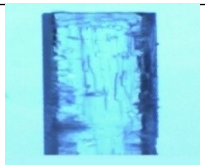	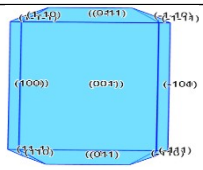

Table S10: Combined ATS + DHA concentrations in MeOH (100%), MeOH (50%), MeOH (20%), MeOH (10%), and MeOH (5) in comparison to the starting concentration at 0 minute.

Time (Minutes)	MeOH (100 %)	MeOH (50%) + DDW (50%)	MeOH (20%) + DDW (80%)	MeOH (10%) + DDW (90%)	MeOH (5%) + DDW (95%)
	µg/mL	µg/mL	µg/mL	µg/mL	µg/mL
0	93.20	103.87	97.03	96.62	82.68
50	93.73	102.05	96.33	94.45	83.94
100	93.37	102.31	95.53	93.95	81.79
150	93.19	101.87	95.05	93.30	80.87
200	92.72	101.47	95.01	92.88	80.68
250	93.66	101.89	94.86	91.83	79.98
300	92.81	101.26	93.66	91.53	79.07
350	93.31	100.50	93.17	90.78	79.09
400	92.90	101.14	91.42	89.83	78.16
450	93.10	100.12	92.13	89.74	77.52
500	93.32	100.60	91.72	89.15	77.60
550	93.25	99.88	91.69	88.22	77.02
600	93.26	100.75	90.51	88.22	76.44
650	92.45	100.11	90.70	87.61	76.78
700	93.25	99.71	90.38	87.61	75.85
750	92.87	100.46	90.33	87.45	75.67
800	93.23	99.55	89.10	86.93	75.88
900	93.29	99.67	90.10	87.16	75.11
950	93.13	99.52	89.78	86.64	75.26
1000	93.71	99.68	89.03	86.14	74.18
1050	93.46	99.39	88.72	85.90	74.92
1100	93.13	98.83	88.22	85.98	74.46
1150	93.65	98.79	88.58	86.27	74.12
1200	93.18	98.86	87.34	85.12	74.70
1250	93.24	98.50	87.67	86.04	74.27
1300	92.75	97.80	87.58	84.91	73.34
1350	92.95	98.06	87.44	84.09	73.44
1400	92.33	97.59	88.02	84.36	72.10
1450	92.98	97.19	87.15	84.80	74.01
1500	92.80	97.06	86.21	83.31	72.72
1550	92.76	96.79	86.03	84.18	72.34

Table S11: ATS and ATS cocrystals/salts PXRD and FTIR measurements after the stress testing

ATS cocrystal	PXRD spectra	FTIR spectra	Note
ATS-ABA	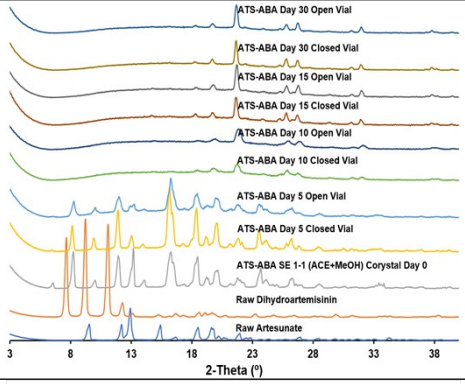	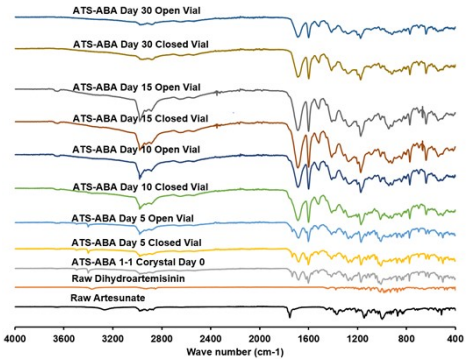	The ATS-ABA cocrystal demonstrates a broken crystal lattice from day 10, as evidenced by the amorphous characteristics observed in the PXRD spectra.
ATS	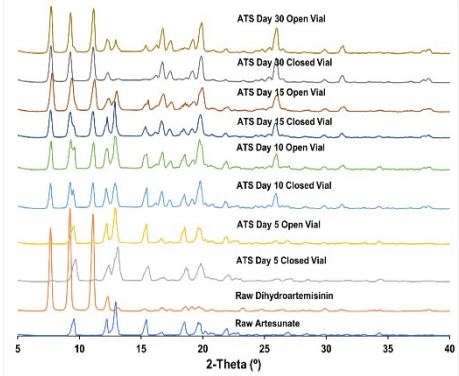	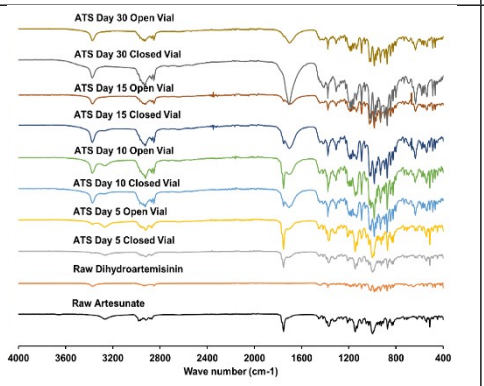	A mixture of raw ATS and DHA was observed, with both spectra present from the 5th day of stress testing, suggesting the transformation of ATS to DHA, similar to HPLC results.
ATS^2-DABCO Form 2	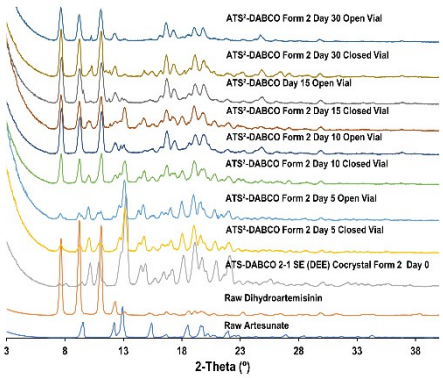	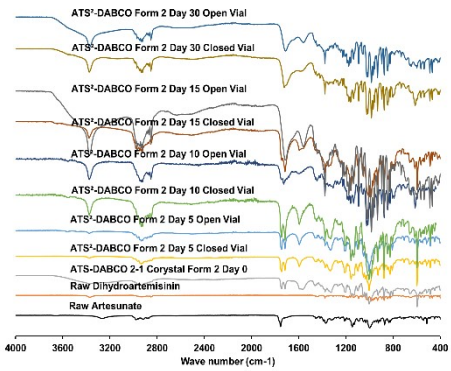	The ATS^2-DABCO Form 2 salt spectra reveal a mixture of ATS, salt, and DHA. The intensity of the DHA spectra increased with the duration of exposure to stress testing, indicating an increased DHA concentration, as shown in Figure S3.
ATS^2-DPE	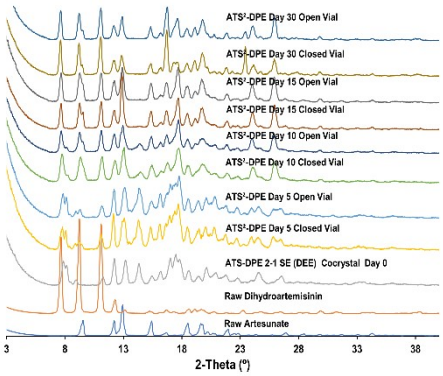	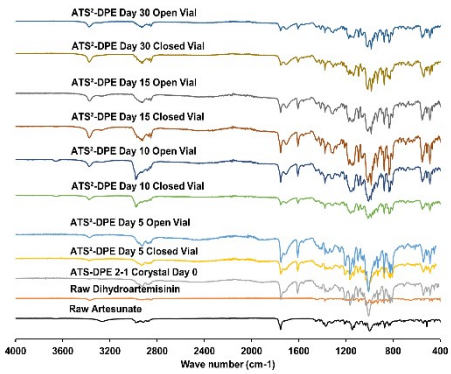	The ATS^2-DPE cocrystal/salt formed a mixture containing ATS, DHA, and ATS^2-DPE, validating the HPLC findings indicating a blend of DHA and ATS.

ATS-PHEN	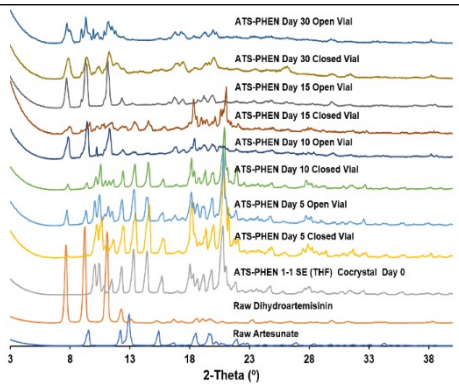	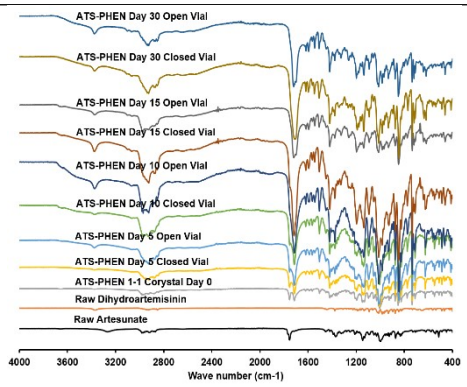	ATS-PHEN degradation suggests a mixture of cocrystal, ATS, and DHA was formed, as some characteristic peaks are present in the spectra.
ATS-URE	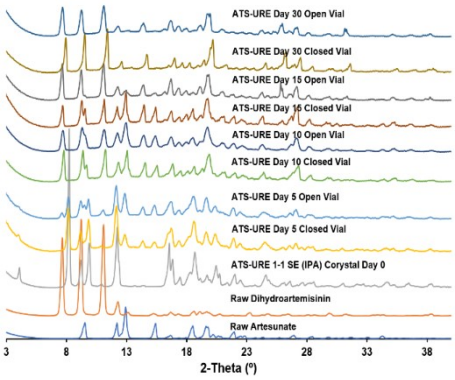	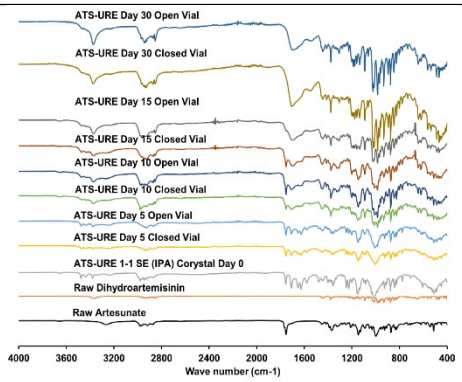	The initial mixture of ATS, cocrystal, and DHA was formed on days 5, 10 and 15 before the apparent transformation of ATS to DHA on day 30 of stress testing.

Table S12: Raw ATS and ATS cocrystals/salts DSC measurements after the stress testing

ATS cocrystal	DSC thermograms
ATS-ABA	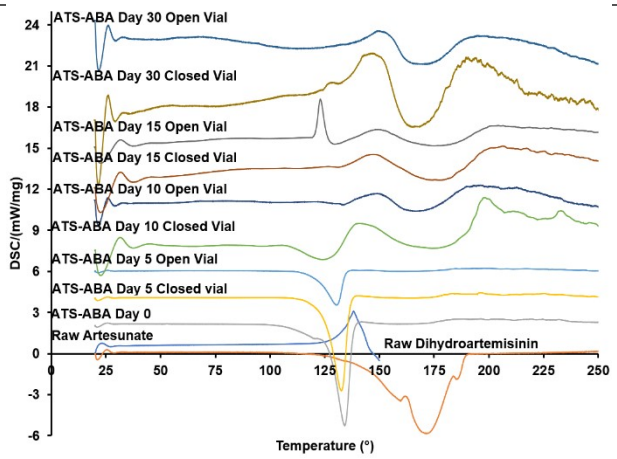
ATS	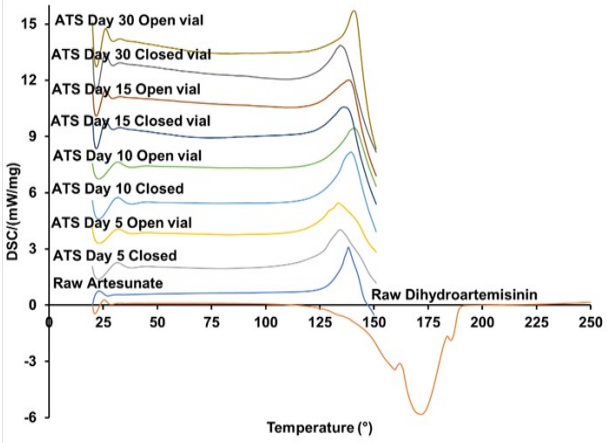
ATS^2-DABCO	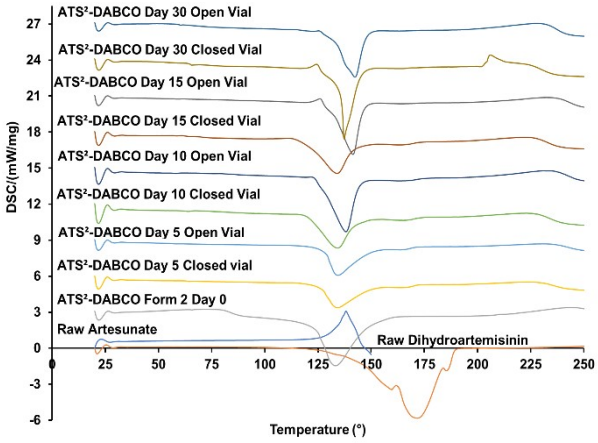

ATS^2-DPE	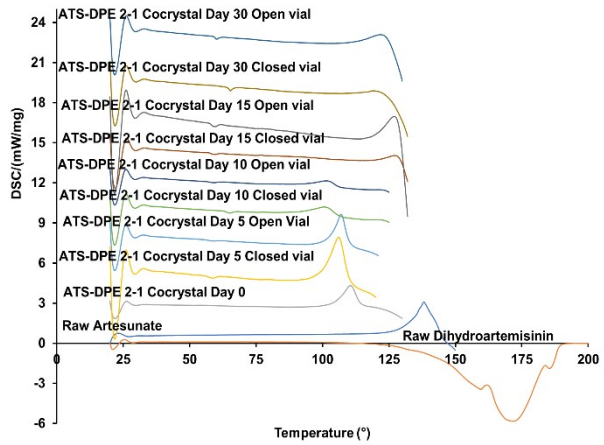
ATS-PHEN	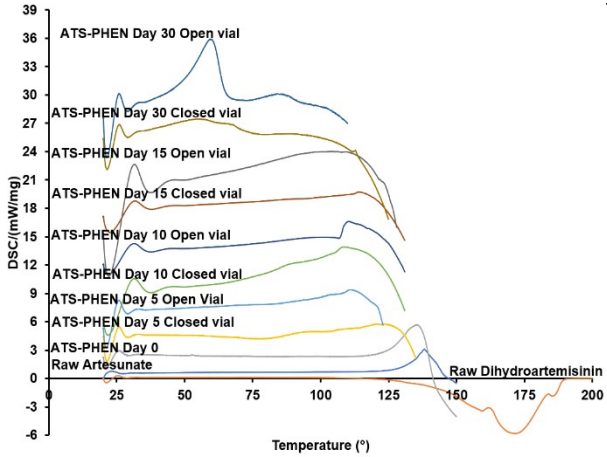
ATS-URE	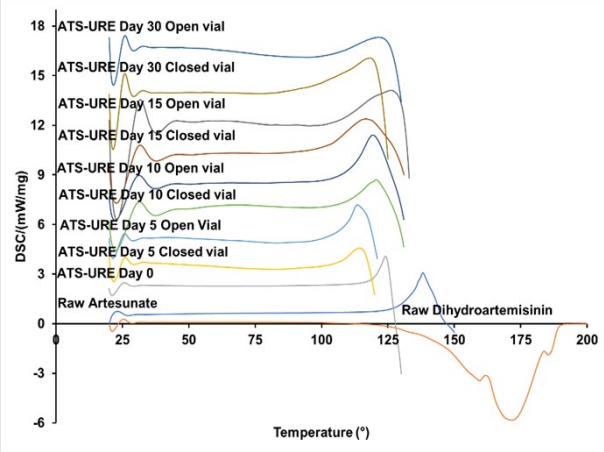

Table S13: Raw ATS and ATS cocrystals/salts TGA measurements after stress testing

ATS cocrystal	TGA thermograms (Closed vials)	TGA thermograms (Open vials)
ATS-ABA	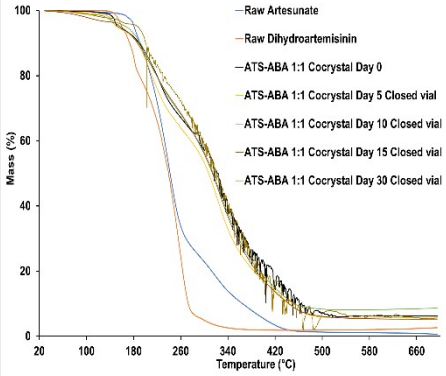	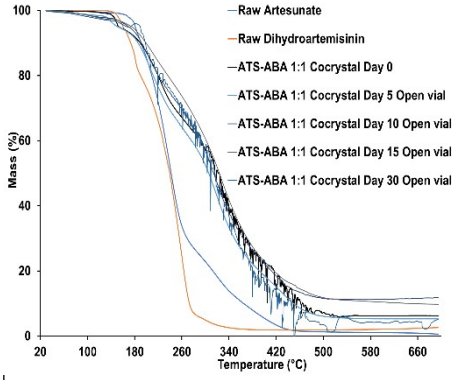
Raw ATS	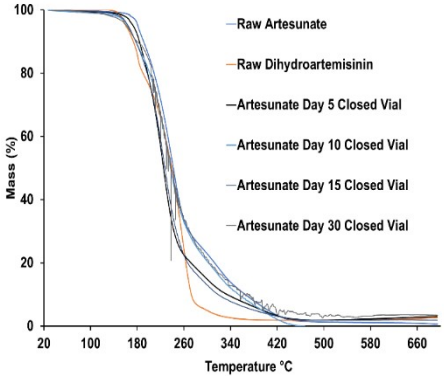	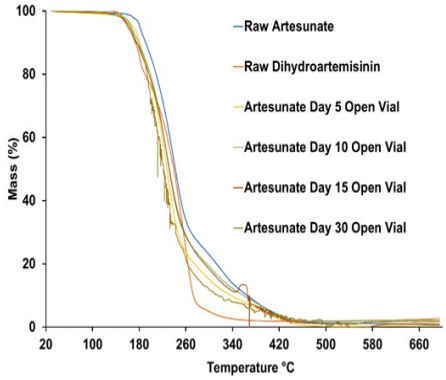
ATS^2-DABCO Form 2	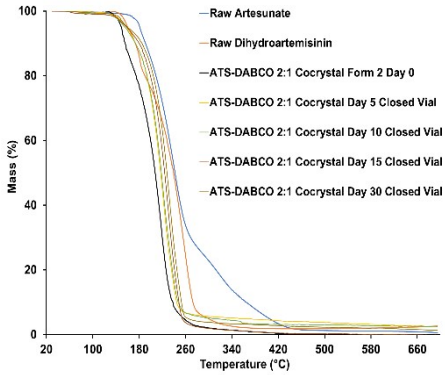	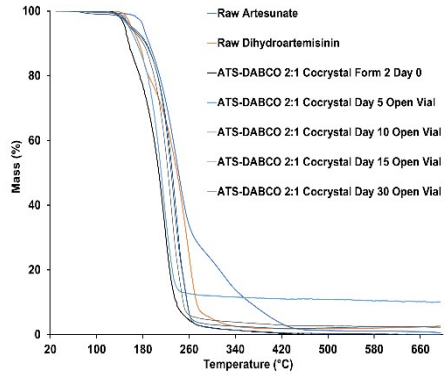
ATS^2-DPE	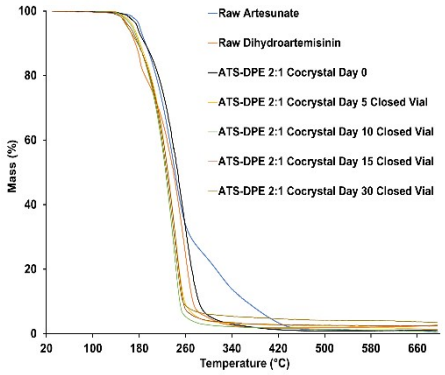	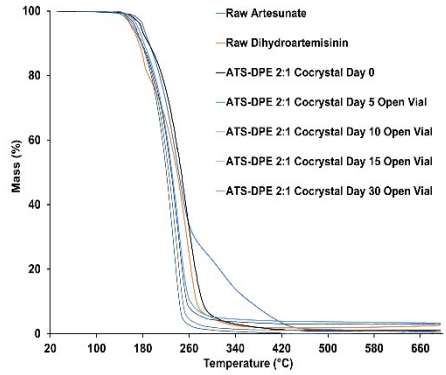

ATS-PHEN	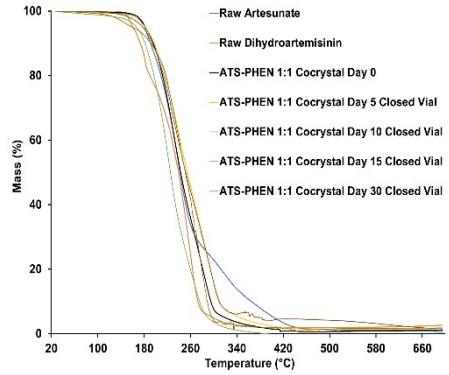	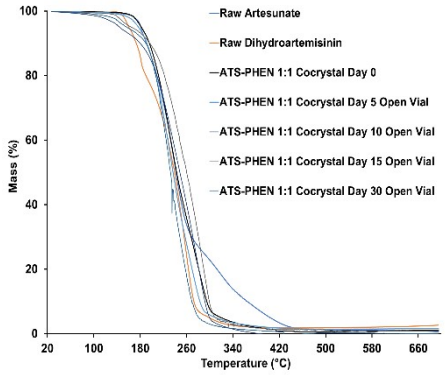
ATS-URE 1:1 SE	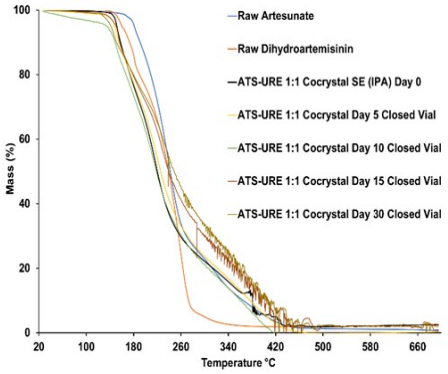	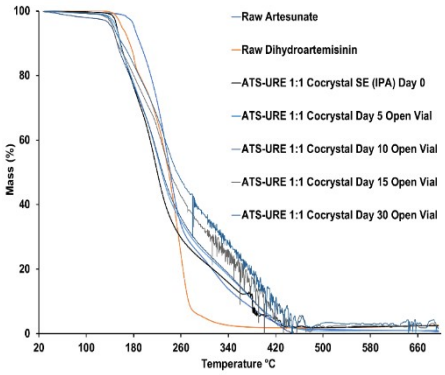

Figure S1: Comparison of (a) DSC and (b) TGA profiles of ATS, DHA, and solids recrystallised from NTM.

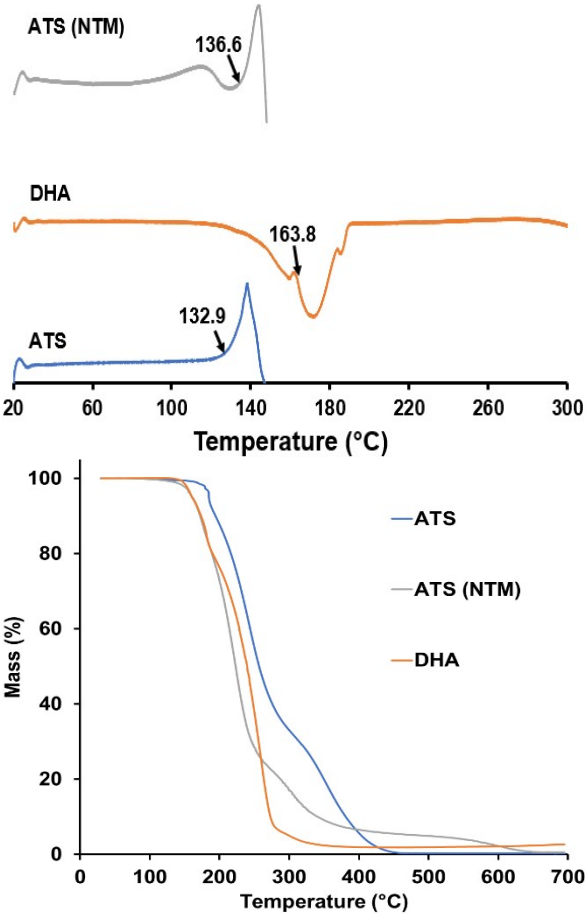

(a) (b)

Figure S2: comparison of FTIR results: (a) raw and recrystallised ATS; (b) solids from NTM with raw ATS and DHA

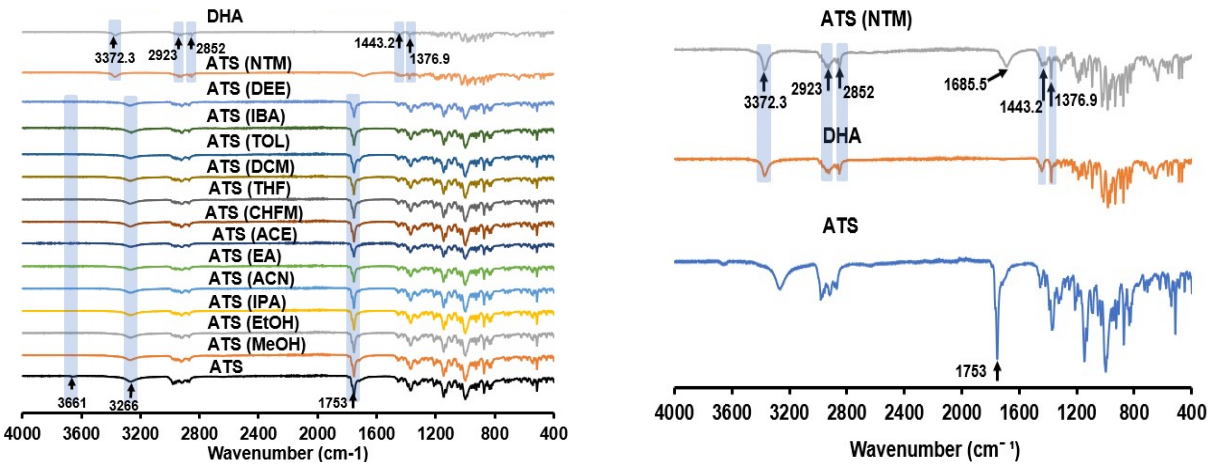

(a) (b)

The FTIR results are consistent with the findings from the PXRD spectra. In all the recrystallized ATS samples, no new polymorphic forms were observed; instead, they retained the crystal packing structure of ATS. This is evidenced by the distinct OH stretching band around 3266 cm^{-1}, the carbonyl group at 1753 cm^{-1}, and the OH stretching vibration in the carboxylic acid observed at 3661 cm^{-1} in concordance with the literature data [4].

Solids recrystallized in NTM exhibited both characteristic bands of DHA and ATS [4, 5]. Transformation to DHA is confirmed by the distinct infrared (IR) absorption bands at 3372.3 cm^{-1} corresponding to the stretching vibration of the O-H group. The presence of symmetric and asymmetric C-H bond vibrations, observed as peaks at 2923 cm^{-1} and 2852 cm^{-1}, respectively, indicates the presence of DHA's methylene (CH2) and methyl (CH3) groups. Furthermore, the appearance of a band at 1443.2 cm^{-1} signifies the bending vibration of the C-H bonds within the -CH2- groups. In comparison, the band at 1376.9 cm^{-1} suggests symmetric bending vibrations of the C-H bonds in the lateral methyl groups. The OH stretching band 3266 cm^{-1} in ATS may have been lost, while the carbonyl group at 1753 cm^{-1} appears to have shifted to 1685.5 cm^{-1}.

Figure S3: Degradation profiles of ATS and its multicomponent salts/cocrystals; a) ATS remaining in 20 % MeOH; b) DHA formed in 20 % MeOH; c) ATS remaining in 10 % MeOH; d) DHA formed in 10 % MeOH

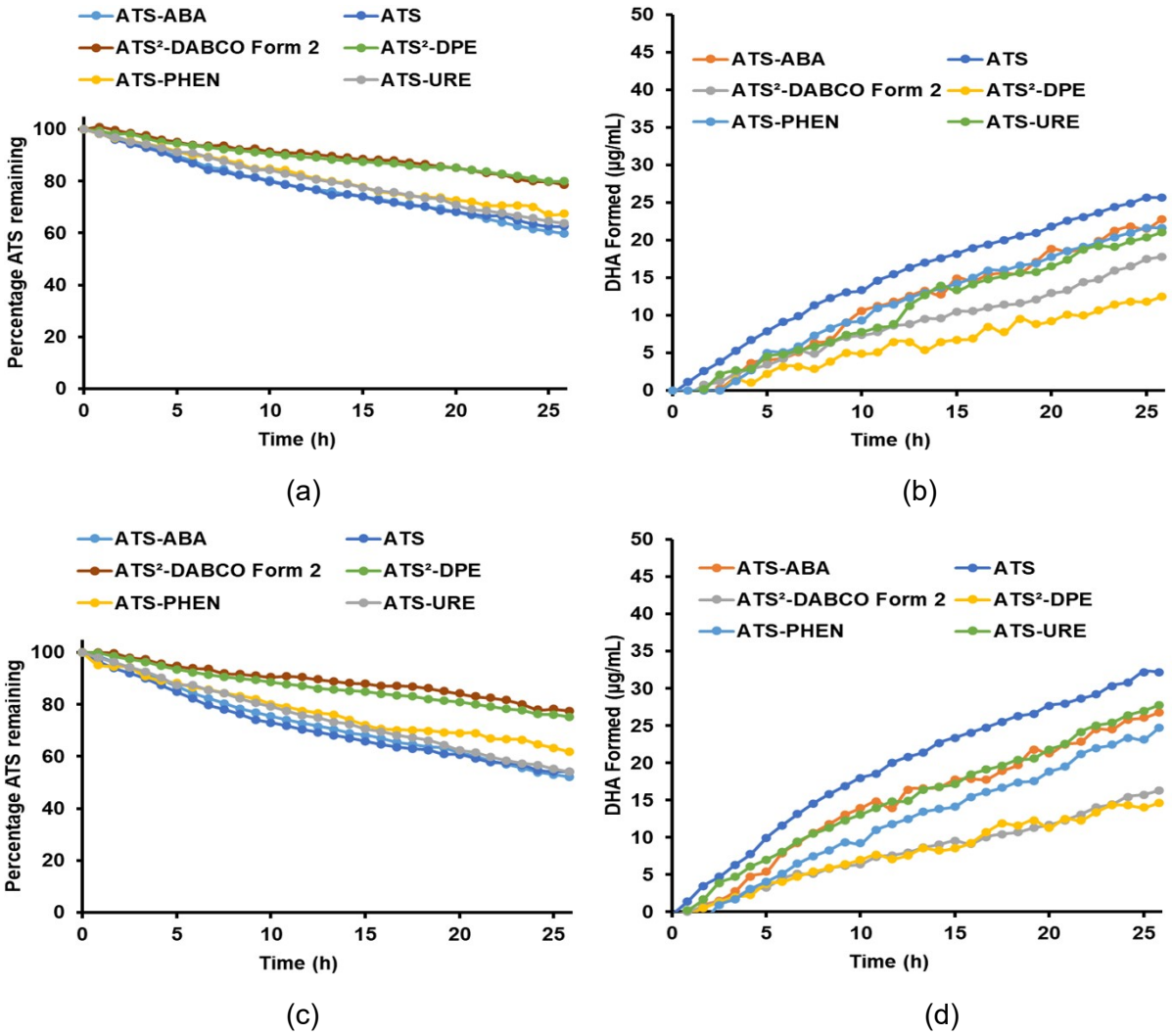

Figure S4: Concentration of DHA formed over time in (a) closed vials; (b) open vials

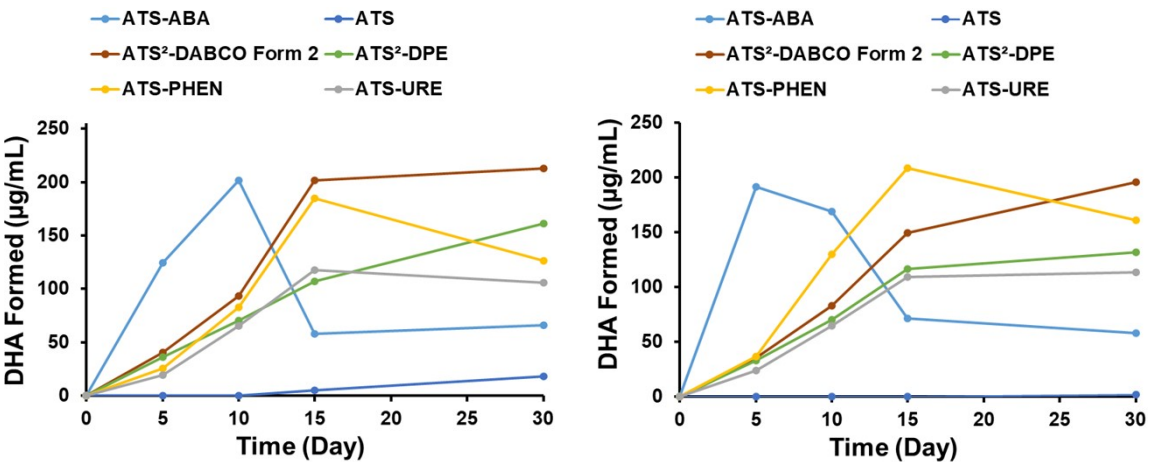

(a) (b)

Figure S5: Comparison of raw ATS and ATS cocrystals/salts' particle size distribution

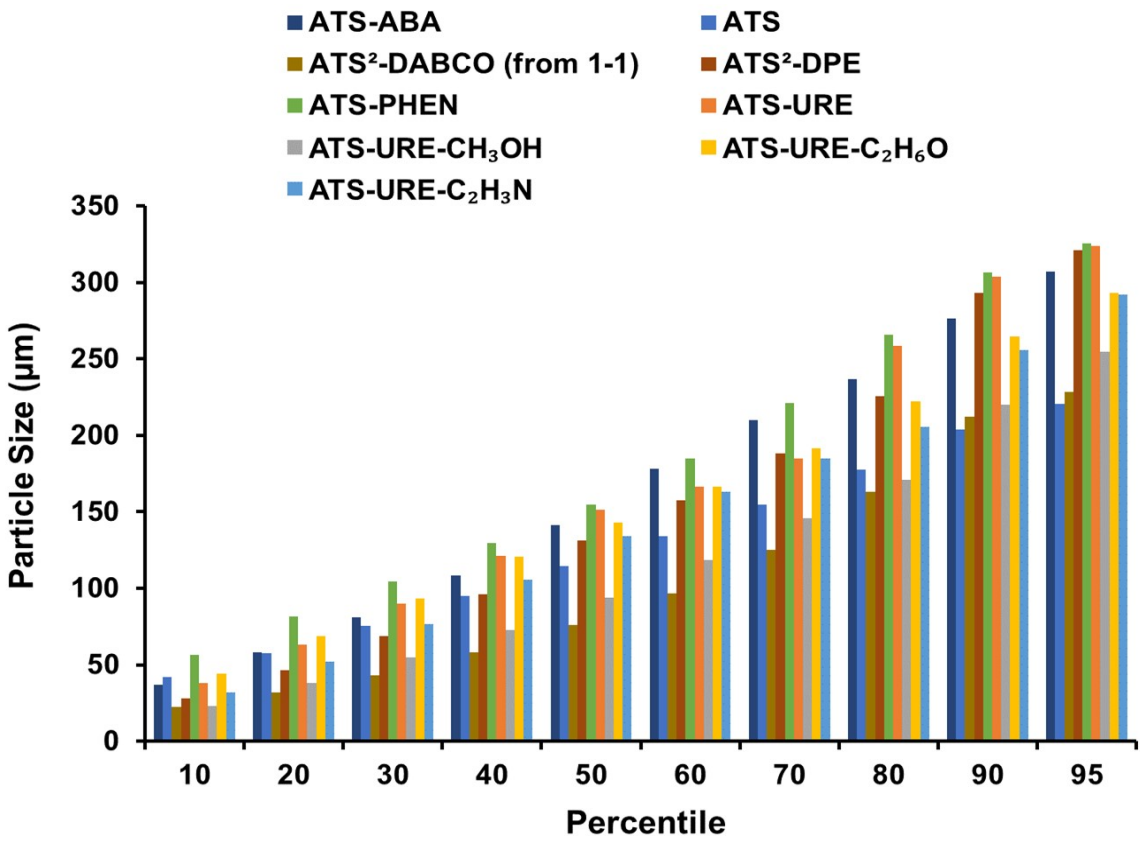

Figure S6: Solid state property of ATS after dissolution and equilibrium solubility assessment in DDW: a) PXRD; b) DSC; c) TGA; d) FTIR

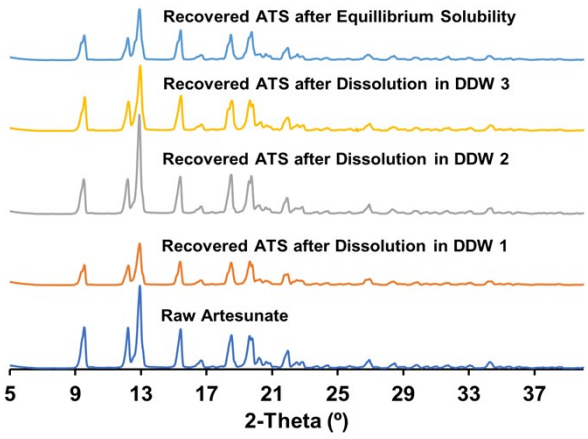

(a)

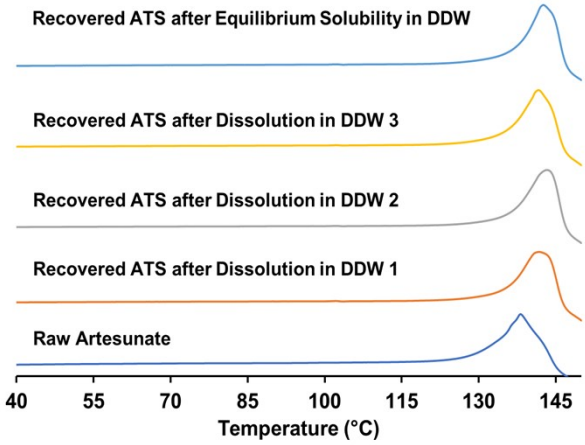

(b)

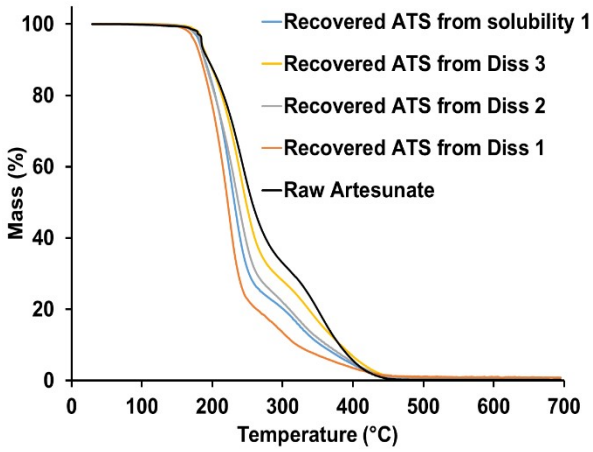

(c)

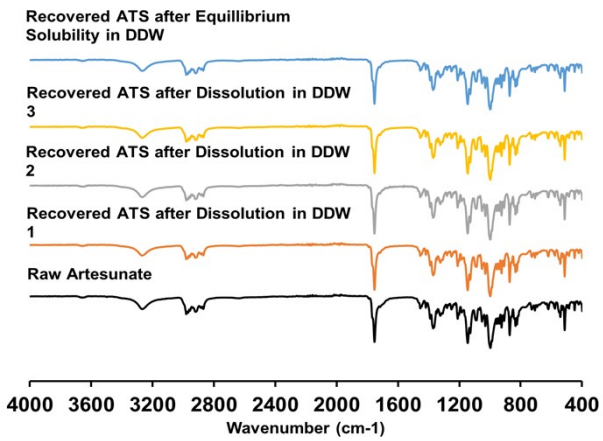

(d)

Figure S7: PXRD results of solid residues after ATS-URE dissolution tests

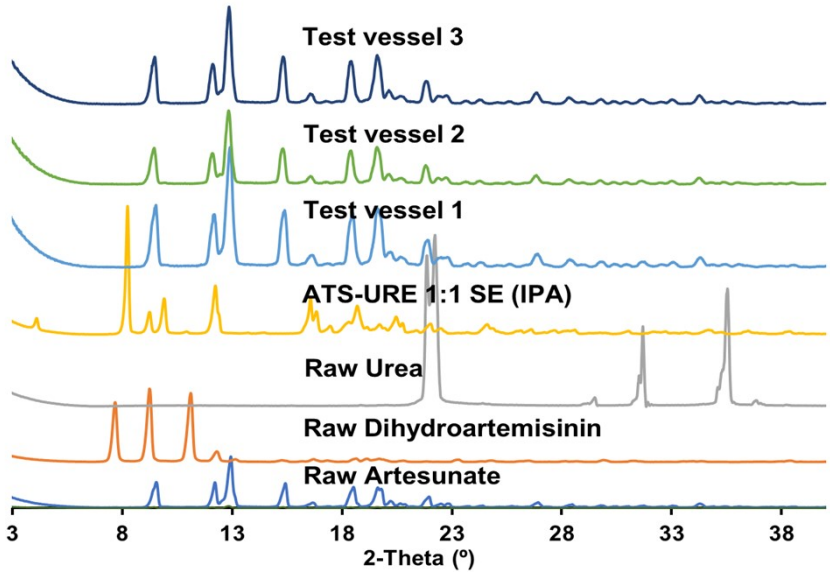

Figure S8: PXRD results of solid residues after ATS-CH_3OH URE-dissolution tests

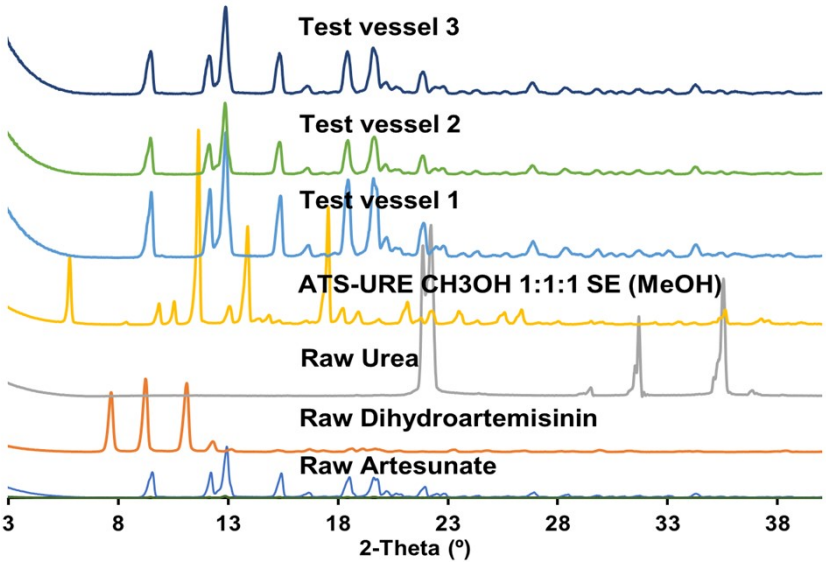

Figure S9: PXRD results of solid residues after ATS-URE-C_2H_6O dissolution tests

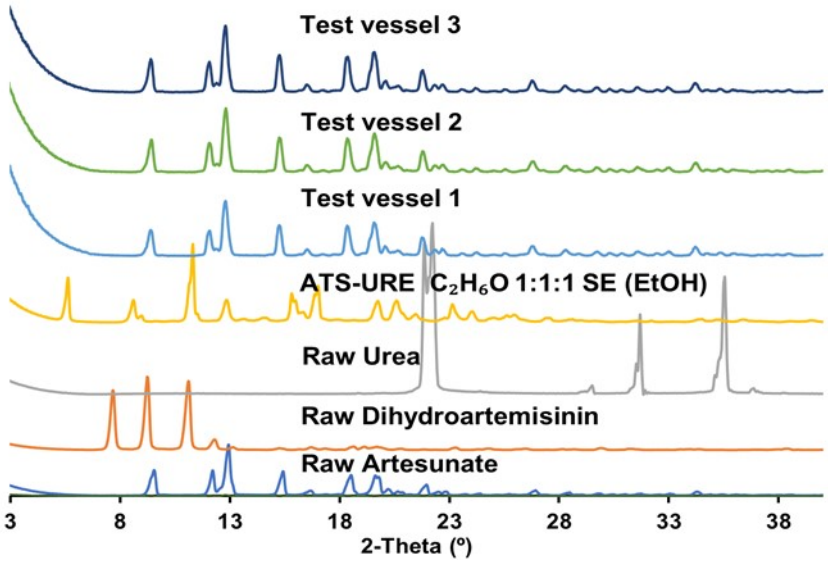

Figure S10: PXRD results of solid residues after ATS-URE C_2H_3N dissolution tests

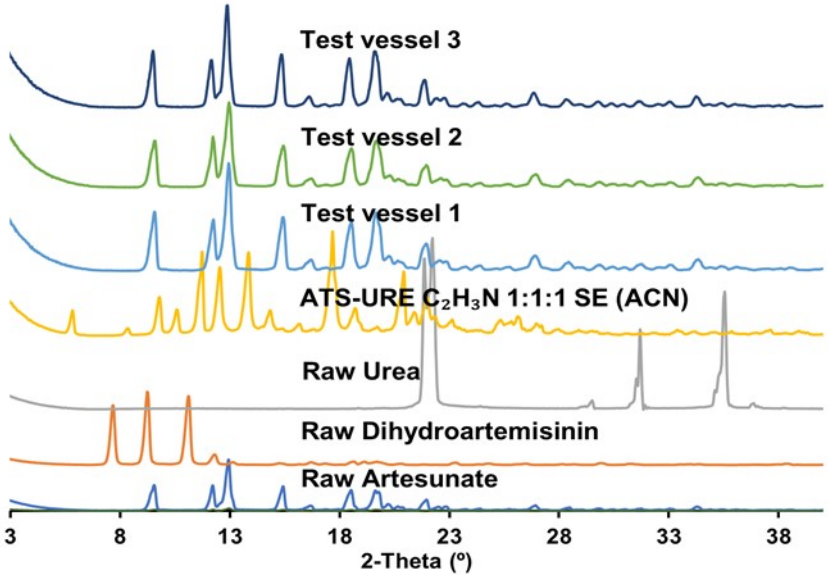

Figure S11: PXRD results of solid residues after ATS-PHEN dissolution tests

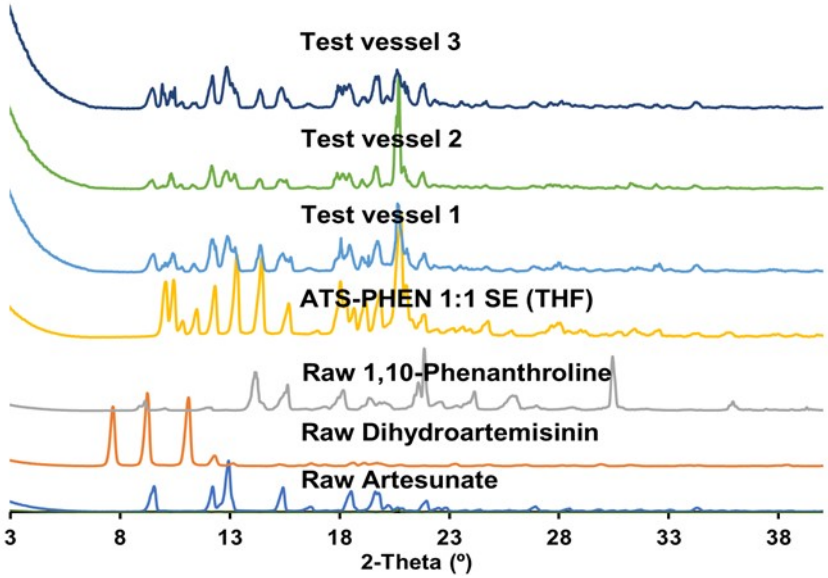

Figure S12: PXRD results of solid residues after ATS-ABA dissolution tests

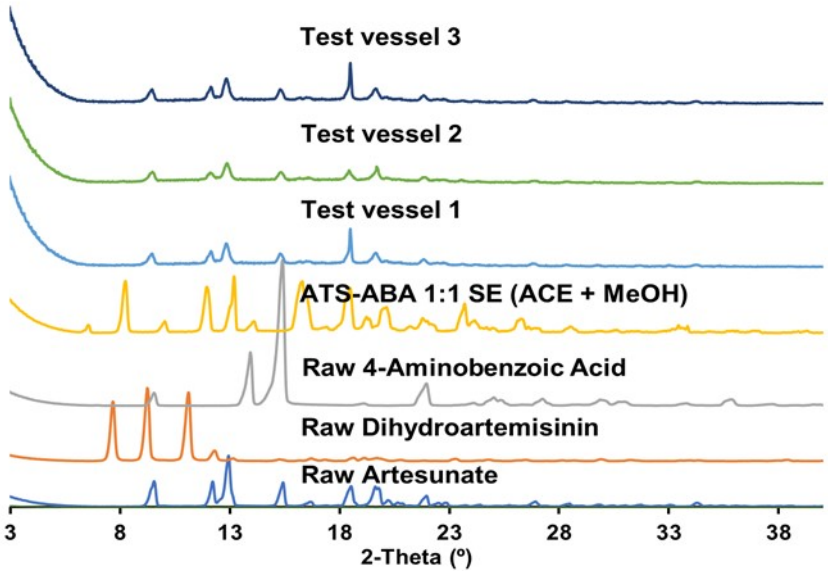

Figure S13: Reconstructed diffraction image of the *0kl* plane for ATS-URE, showing the marked diffuse streaks formed along the **c*** direction. The data were indexed with orthorhombic unit cell parameters *a* = 5.3403(2) Å, *b* = 9.5836(3) Å, *c* = 42.6545(17) Å.

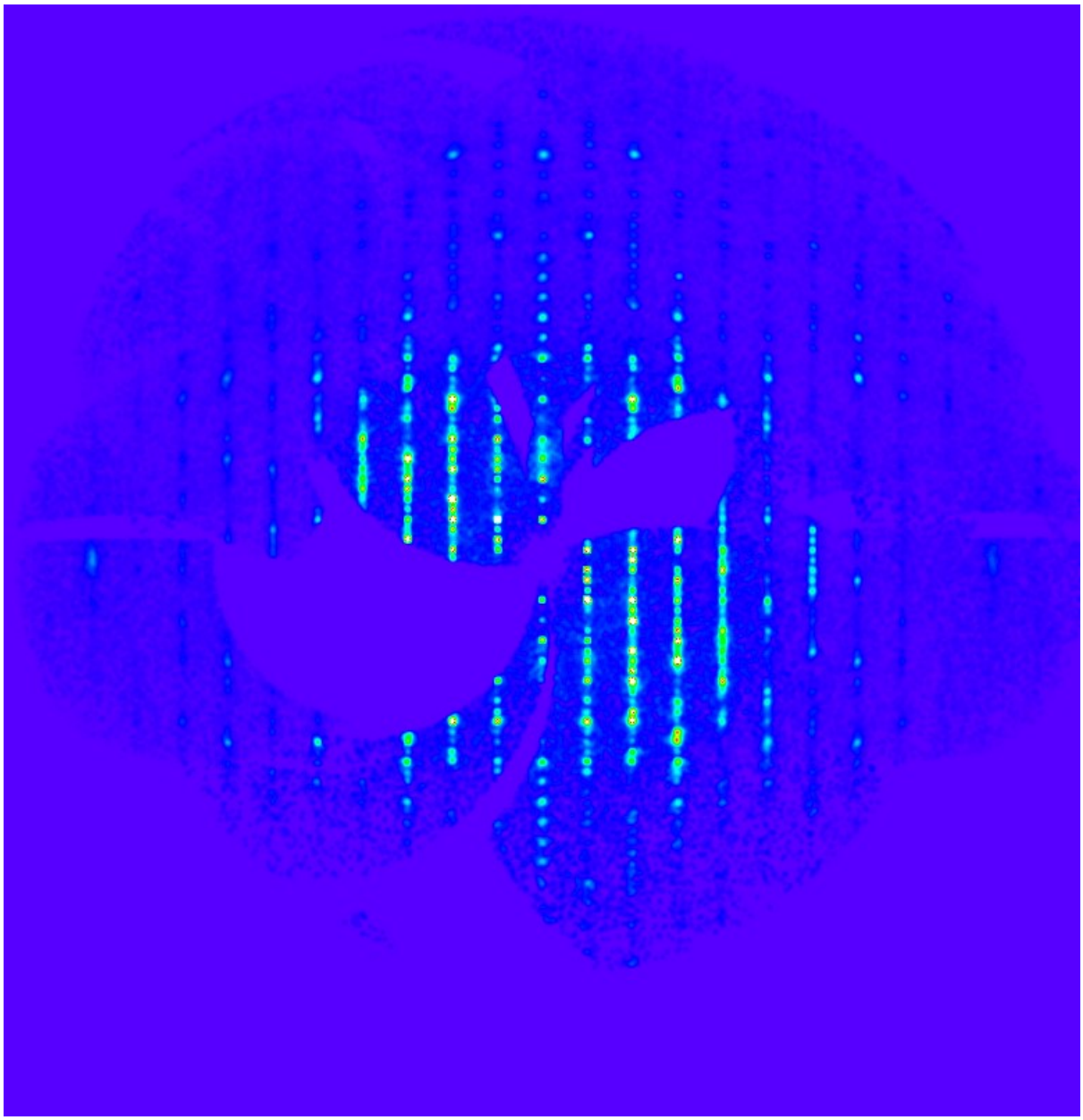

Figure S14: Difference Fourier map calculated for ATS^2-DABCO form 2 at the 0.25 *e*/$Å^3$ level. The negative density around O2, C12 and O13 (red) indicates the possibility that a minor disorder component is present with the ring system broken up. The positive density peaks (green) did not reveal a clear structural model for the product.

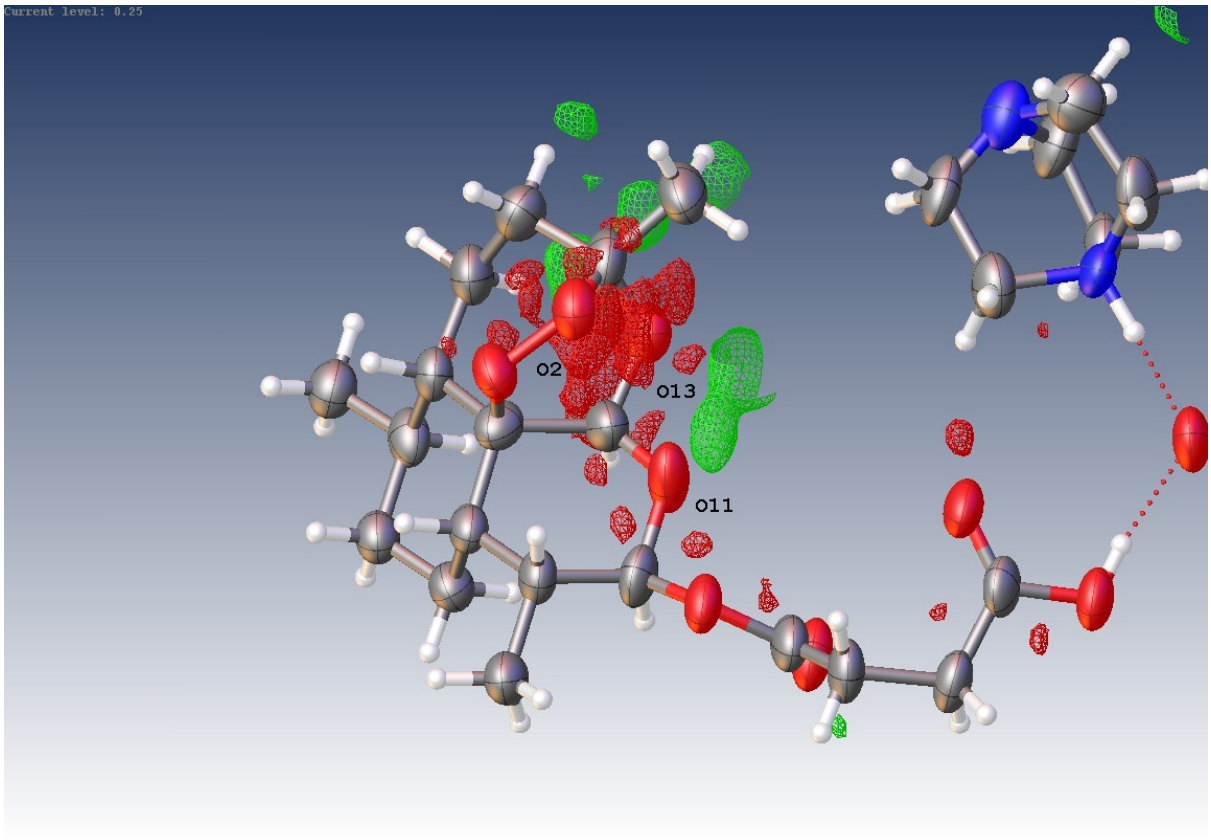

References

1. Silverstein, R.M., G.C. Bassler, and T.C. Morrill, *Spectrometric identification of organic compounds* 1991, Singapore: John Wiley & Sons, Inc. 100-128.
2. Samie, A., G.R. Desiraju, and M. Banik, *Salts and Cocrystals of the Antidiabetic Drugs Gliclazide, Tolbutamide, and Glipizide: Solubility Enhancements through Drug–Coformer Interactions.* Crystal Growth & Design, 2017. **17**(5): p. 2406-2417.
3. Yang, S.-Y., et al., *Pharmaceutical cocrystals and salts of enrofloxacin: Structure and properties.* Journal of Molecular Structure, 2022. **1265**: p. 133335.
4. LUO, B., et al., *Synthesis, Characterization and Antibacterial Activities Study of a Pharmaceutical Cocrystal of Artesunate and 4,4´-Bipyridine.* CHINESE JOURNAL OF STRUCTURAL CHEMISTRY, 2020. **39**(9): p. 1633-1638.
5. Circioban, D., et al., *Thermal stability and kinetic degradation study for dihydroartemisinin.* Journal of Thermal Analysis and Calorimetry, 2020. **142**(5): p. 2131-2139.